Journal of Fluids and Structures (1993) **7**, 423–455

DIMENSIONLESS PARAMETERS IMPORTANT TO THE PREDICTION OF VORTEX-INDUCED VIBRATION OF LONG, FLEXIBLE CYLINDERS IN OCEAN CURRENTS

J. K. VANDIVER

Department of Ocean Engineering, Massachusetts Institute of Technology, Room 5-222, Cambridge, Massachusetts 02139, U.S.A.

(Received 5 July 1991 and in revised form 6 May 1992)

Case studies drawn from 17 years of field and laboratory experiments are used to demonstrate and explain why the flow-induced vibration of long cylinders in ocean currents varies from single mode lock-in to broad-band random vibration. It is shown that, with careful consideration of a few dimensionless parameters, the range of observed behavior is predictable. New interpretations are given to the significance of familiar parameters such as mass ratio and reduced damping. In addition, the fractional variation in flow velocity over the length of the cylinder and the number of natural frequencies within the bandwidth of the vortex-shedding frequencies are shown to be of considerable importance.

When consideration of the above parameters reveals that multiple mode response without lock-in is likely to occur, then hydrodynamic damping is revealed to have a powerful influence on dynamic response, and the simple product of the total damping ratio and the mode number allows one to anticipate the whole range of response behavior, from the wave propagation properties of infinite length cables to the standing wave features of short cylinders.

1. INTRODUCTION

THE VORTEX-INDUCED VIBRATION of a long flexible cylinder, such as a mooring cable or a deep water petroleum production riser, depends on many dimensionless parameters acting in concert. The prediction of the vibration requires that one weigh the relative influence of each parameter and estimate the probable outcome. A sequential approach is used in this paper, beginning with the determination of whether or not lock-in is possible. The most important parameters in this determination are shown to be: the shear fraction, $\Delta V/V_{max}$, and the number of resonant natural modes, N_s, within the shear excitation bandwidth. Also important are the reduced damping, S_G, the mass ratio, μ, and the turbulence intensity. When it is determined that lock-in is likely, then it is possible to turn to a large established literature to make precise estimates of response amplitudes (Griffin & Ramberg 1982).

When lock-in is not the predicted response, there are three principal causes: (i) the reduced damping is sufficiently large that no significant motion results; (ii) the vortex-shedding frequency does not correspond to any natural frequency; (iii) the excitation bandwidth includes the natural frequencies of more than one mode, resulting in a multi-moded response with random vibration characteristics.

Of the three reasons the third, multi-moded behavior, is the least well understood and is of considerable practical importance. This subject is examined in detail in this paper. In this case $\Delta V/V_{max}$ and N_s are important parameters, in that they are reliable

0889–9746/93/050423 + 33 $08.00

indicators of multiple mode nonlock-in response. When multiple mode nonlock-in response is to be expected, then a parameter characterizing the expected wave propagation properties of the cylinder is useful. This "wave propagation parameter" is $n\zeta_n$, the product of the mode number and the total modal damping ratio, ζ_n; the total modal damping ratio, includes the hydrodynamic contribution. This wave propagation parameter is recognized in the field of mechanical vibration by several names. It can be derived by considering the attenuation of a wave travelling the length of the cylinder or it can be derived by calculating the ratio of the half-power bandwidth of mode n to the separation in frequency between modes. Thus it is a measure of what is known as modal overlap. Regardless of the way one derives this parameter, it is useful in anticipating dynamic behavior, which may vary from cylinders with infinite-length properties to those with standing waves and clearly distinguishable mode shapes.

2. EVALUATING CONDITIONS FAVORABLE TO LOCK-IN

By the mid-1970s a great deal of laboratory-scale research had been completed by many investigators on fixed and moving cylinders in fluid flows. Concepts such as lock-in, correlation length, and drag coefficient dependence on response amplitude were quite well developed. Missing at the time were systematic experiments on long, flexible cylinders which could rationally extend the observations made in laboratory scale tests to field applications of much larger scale.

2.1. The Early Castine Experiments

In the summers of 1975 and 1976, the author, with the sponsorship of the Office of Naval Research, conducted experiments in a tidal flow at Castine, Maine. Most of the cylinders tested were synthetic fiber, or wire cables, 75 feet (22·9 m) in length with diameters varying from $\frac{1}{4}$ to $\frac{5}{8}$ in. (0·64 to 1·59 cm). Flow velocity was quite spatially uniform and varied slowly with time from 0·50 to 2·50 ft/s (0·152 to 0·762 m/s).

The typical vibration response was single mode lock-in with response amplitudes of ±1 diameter at the antinodes. At certain flow velocities there were occurrences of a lower amplitude random vibration response which was called nonlock-in behavior (Vandiver & Mazel 1976). The Reynolds number range for these tests was from 800 to 10,000, and the reduced damping was very low. The observed response was rather insensitive to variations in Reynolds number as well as to large amounts of surface roughness, due typically to the cable braid or the helical lays of rope.

An initially inexplicable, but ultimately significant, event occurred. On one occasion, a plastic-jacketed wire rope 0·280 in. (0·71 cm) in diameter and 900 ft (274 m) in length was stretched across the tidal basin from two points of land. The submerged portion of the cable was approximately 500 ft (152 m) long and was exposed to flow which varied approximately 20% along the length. In spite of the sheared flow velocity profile, lock-in occurred at approximately the 50th mode. Response amplitudes of $\pm\frac{1}{2}$ to ±1 diameter were observed. This established that lock-in is possible at very high mode numbers in the presence of a mild sheared flow.

2.2. Castine, 1981

A much more ambitious experiment, sponsored by ONR, the U.S. Geological Survey and a consortium of industry sponsors, was conducted in the summer of 1981 at the same site, at Castine, Maine. The experiment lasted 6 weeks and involved eight people

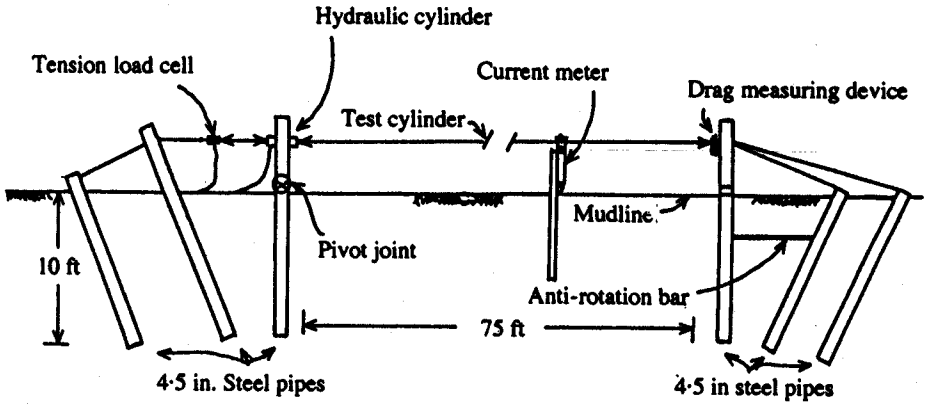

Figure 1. Castine experimental setup, 1981.

in the field with the research vessel Edgerton from the MIT Sea Grant Programme. The experimental set-up is shown in Figure 1.

Two test cylinders were used in the experiments. The first was a cable 75 ft (22·86 m) in length, $1\frac{1}{4}$ in (3·18 cm) in diameter, containing seven biaxial pairs of accelerometers. In the experiments, tension, acceleration, current and mean drag coefficient were measured. This cable was also pulled inside of a 1·625 in. (4·13 cm) diameter steel pipe, which was then used as the second test cylinder. The pipe was selected to provide a cylinder with a significantly different mass ratio and a non-negligible bending rigidity. Properties of the test cylinders are given in Table 1.

The primary objectives of this field experiment were to (i) measure mean drag coefficients under field conditions and compare them to the very high values observed under laboratory conditions, (ii) determine the differences in behavior of cables and pipes with significant differences in bending stiffness and mass ratio, and (iii) test cable behavior with attached lumped masses. The behavior with lumped masses is reported in Griffin & Vandiver (1984).

The field measurements of drag coefficients are presented in Figures 2 and 3

TABLE 1

Mechanical properties and dimensions of test cylinders

Cable specifications	
Length	75·0 ± 0·1 ft (22·86 ± 0·03 m)
Diameter	1·25 ± 0·02 in (3·175 ± 0·051 cm)
Weight in air	0·7704 lb/ft (1·146 kg/m)
Specific gravity	1·408
Pipe specifications	
Length	75·0 ± 0·02 ft (22·86 ± 0·006 m)
Outside diameter	1·631 ± 0·003 in. (4·143 ± 0·008 cm)
Inside diameter	1·493 ± 0·003 in. (3·792 ± 0·008 cm)
Weight in air, including the weight of the internal cable	2·001 lb/ft (2·978 kg/m)
Weight per unit length, including cable and trapped water	2·236 lb/ft (3·328 kg/m)
Specific gravity of pipe with cable and trapped water	2·40
Measured bending stiffness, EI	$(3{\cdot}016 \pm 0{\cdot}05) \times 10^6$ lb in^2 $(8{\cdot}66 \pm 0{\cdot}14) \times 10^3$ N m^2

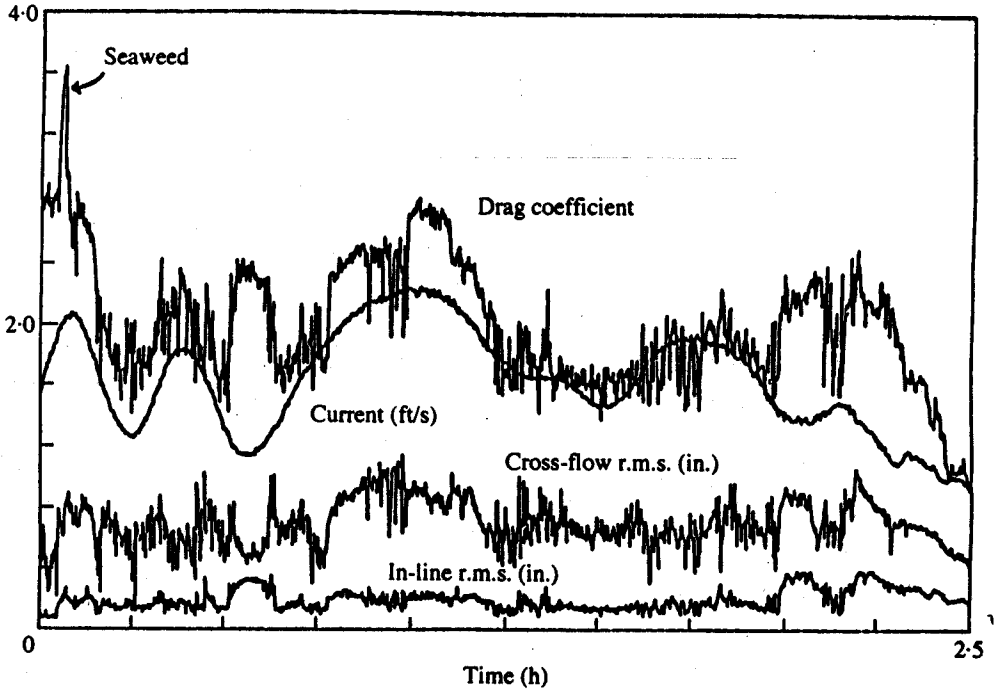

Figure 2. Drag coefficient (C_D), current, r.m.s. displacement at $L/6$, for the pipe, T from 670 to 920 lb (2980 to 4092N). C_D error ± 10% at 2 ft/s (0·61 m/s), ±15% at 1 ft/s (0·305 m/s).

(Vandiver 1983). Figure 2 shows the current speed and the drag coefficient for the pipe measured over a period of 2·5 h. The data is moving average data. A moving average is a very simple low pass digital filter. In this case the data was sampled at 120 Hz. A moving average is constructed by capturing 8·53 s of data (1024 data points) and computing an average. The time window is then incremented by 1024 data points and a new average is computed. The entire time series is averaged in this way and the resulting time series is plotted. The total number of data points is reduced by the factor 1024, and the resulting time history has only very low frequency components.

Also shown in the figure are the r.m.s. vibration amplitudes observed in the

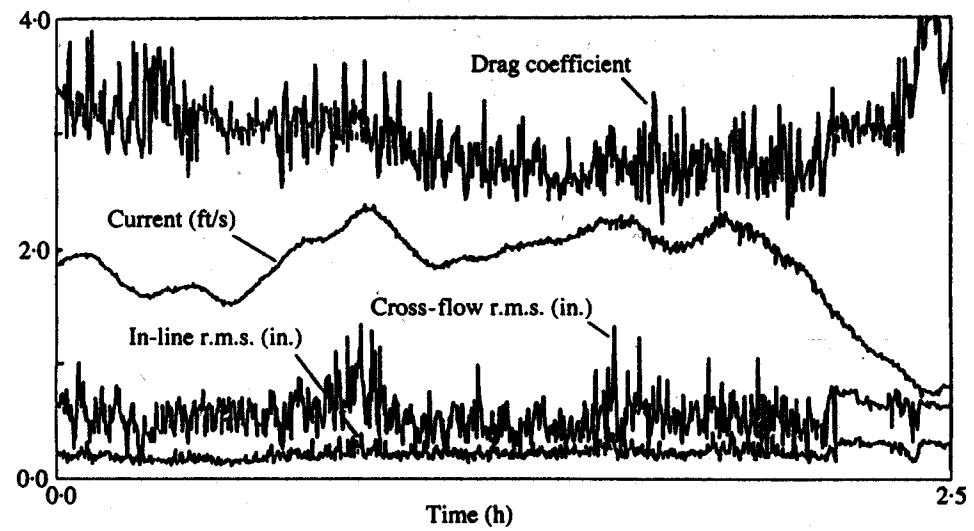

Figure 3. C_D, current, r.m.s. displacement at $L/6$, for the cable, T from 320 to 600 lb (1423 to 2669 N). C_D error bound +0%, −20%.

cross-flow vibration direction and the in-line vibration direction at one location on the cylinder. The location was at $\frac{1}{6}L$, or one-sixth of the length from one end of the cylinder. The r.m.s. calculation was made on the same 1024 point window as the moving average calculation of drag coefficient and current.

In Figure 2, for the pipe, the data reveals periods or plateaus of high drag coefficient adjacent to periods of relatively low drag coefficient. The plateaus are at times of lock-in with individual modes which are indicated in the figure; for example, 2nd and 3rd mode. At these times the natural frequency of the cylinder for the mode indicated, coincided with the vortex-shedding frequency. The valleys in drag coefficient occurred at times when the flow velocity was such that wake synchronization could not occur. At these times vibration still occurred, but with lower r.m.s. amplitudes and with broader band random vibration characteristics than occurred during single mode lock-in. Under lock-in conditions, the drag coefficients were greater than two times the value of a similar non-moving, rigid cylinder at the same Reynolds number.

The reported in-line and cross-flow r.m.s. response measurements shown in the figures are plotted for only one location, $\frac{1}{6}L$. The response amplitude at this location is influenced by mode shape. For example this location would show zero response for vibration in the sixth mode, and would show maximum antinode response for the third mode. One must not, therefore, attempt to draw quantitative conclusions about response amplitude from these r.m.s. plots without taking mode shapes into consideration. Modal response amplitudes have been evaluated for these experiments (Vandiver & Jong 1987).

Figure 3 is also a 2·5 h record, but for the cable. Again, very high drag coefficients are observed. However, there is one remarkable difference between the cable data and the data shown for the pipe in Figure 2. There are no obvious plateaus and valleys in the drag coefficient. There are no clear demarcations between periods of lock-in and nonlock-in behavior. That difference in mass ratio between the pipe and the cable was the cause of the difference in response, did not become clear until a few years later. This is discussed in the next section.

The drag coefficient data deserve further explanation. They are least accurate at low flow speeds. This is due to absolute errors in zeroing the load cell under field conditions. These absolute errors lead to large percentage errors at low flow speeds when the drag force is small. For the cable data, the large increase in measured drag coefficient at the end of the run is due to such an offset error. The error bounds are given with the figure titles.

2.3. The Importance of Mass Ratio

The mass ratio is $m/\rho_f D^2$. It is $\pi/4$ times the ratio of the mass per unit length of the cylinder (m) to the mass per unit length of the displaced fluid ($\pi\rho_f D^2/4$). Some authors include the added mass when reporting the mass per unit length. This should be avoided because the added mass is not constant, as will be discussed below.

Figure 4 (Chung 1987) shows data from a variety of sources: Griffin & Ramberg (1982), Tsahalis (1984) and Koch (1985). Response amplitude is plotted versus reduced velocity for a variety of cylinders with different mass ratios. The reduced velocity, V_R, in this figure is based on the in-air natural frequency, which to sufficient accuracy is the same as the *in vacuo* value. In other words an added mass coefficient of zero has been used. The data for a mass ratio of 0·78 (specific gravity = 1·0) is for first mode vibration of a neutrally buoyant aluminum tube, 120 mm diameter, 9·93 m long, immersed in water (Koch 1985).

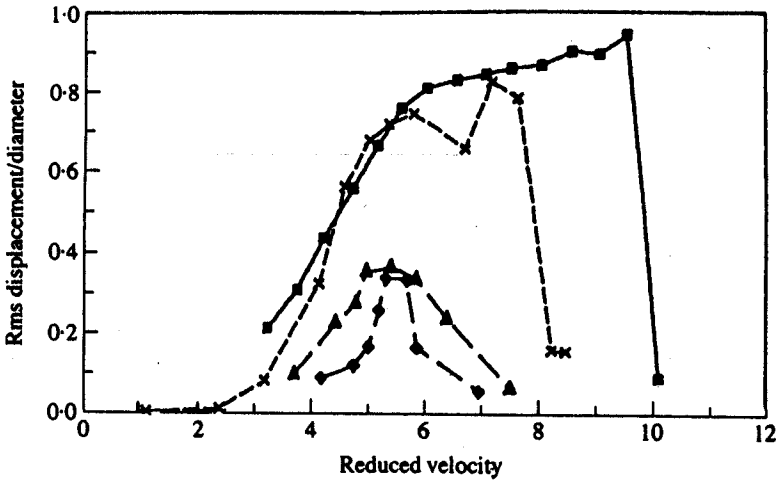

Figure 4. R.m.s. displacement versus reduced velocity for various mass ratios (Chung 1987): □, $m/\rho_f D^2 = 0{\cdot}78$, $S_G = 0{\cdot}015$; ×, $m/\rho_f D^2 = 1{\cdot}77$, $S_G = 0{\cdot}03$; Δ, $m/\rho_f D^2 = 3{\cdot}8$, $S_G = 0{\cdot}6$; ◇, $m/\rho_f D^2 = 34$, $S_G = 0{\cdot}5$.

The remarkable conclusion that one can draw from this figure is that low mass ratio cylinders have a much broader lock-in range than high mass ratio ones, when the reduced velocity is computed using the measured flow speed and the *in-air natural frequency*, not the observed vibration frequency. This property is the key to understanding the difference between the response characteristics of the pipe and the cable in the 1981 Castine experiments.

Large amplitude, self-excited, lock-in occurs, if and only if, there is a synchronization of the periodic formation of vortices in the wake and resonant motion of the cylinder. The range of frequencies which permit this synchronization is governed by two factors. One is the response bandwidth of the resonant peak of the oscillator, which is given approximately by twice the damping ratio, multiplied by the natural frequency: $2\zeta_n\omega_n$. For example, a resonant mode with 1% damping will have a resonant bandwidth of approximately 2% of the natural frequency. For a fixed natural frequency this is much too small to explain the wide lock-in bands exhibited in Figure 4. The second factor is the tolerance of the wake synchronization process to variations in reduced velocity resulting from changes in flow speed. Hereafter, this will be referred to as the lock-in bandwidth of the wake.

Driven cylinder experiments have shown that for a *fixed vibration frequency*, and favorable cross-flow vibration amplitudes, the range of flow velocity, and therefore reduced velocity, that permits wake synchronization is narrow. The typical lock-in bandwidth of the wake, expressed in reduced velocity terms is approximately 5·0 to 6·5, or about a 25% variation. The precise limits of this range also depend on Reynolds number, turbulence intensity, roughness and the amplitude of vibration of the cylinder. Taking all of these into consideration, however, the conclusion is the same; the lock-in bandwidth of the wake is much narrower than the lock-in range exhibited by low mass ratio cylinders, such as some of those shown in Figure 4. Therefore, the only remaining explanation of the wide resonant lock-in range shown in the figure for some cylinders is that the cylinder resonant response frequency is not constant, but must be increasing, as the flow velocity increases. Close inspection of response frequency data for low mass ratio cylinders, reveals that over the lock-in range the response frequency increases with the flow velocity. This effect is most pronounced for the lowest mass ratio cylinders.

The rise in the resonant response frequency with flow speed is due to the variation in the added mass coefficient over the lock-in range. There is driven-cylinder data (Sarpkaya 1977) to support this hypothesis. His data reveals that at an amplitude-to-diameter ratio of 0·5 the added mass coefficient decreases sharply from values of 5·5 to −0·8, as the reduced velocity varies from 2·5 to approximately 5·5. The added mass coefficient then rises slowly to about −0·5 as the reduced velocity increases to the limits of the data at 8·0. This phenomenon is similar for a wide range of vibration amplitudes. The consequence of importance in the context of the lock-in bandwidth is that, if the added mass decreases with increasing reduced velocity, then the natural frequency of the cylinder will increase. This allows the lock-in region to persist to higher values of flow speed.

The concept of a negative added mass deserves some explanation, because it seems contrary to the usual concept of added mass. As vortices are shed from a sinusoidally oscillating cylinder, the fluid exerts forces perpendicular to the mean flow direction. These lift forces have a phase angle with respect to the cylinder motion. That part of the fluid force in phase with the velocity of the cylinder puts energy into the cylinder, while force exactly opposing the velocity produces damping of the cylinder motion. Fluid force in opposition to the acceleration would typically be associated with a positive added mass. That portion in phase with the acceleration would yield a negative added mass coefficient. Hence a negative added mass simply reflects the sign of the fluid force on the cylinder being in phase with the acceleration.

High mass ratio cylinders are less affected by changes in the added mass coefficient, because the added mass is a lower percentage of the total mass per unit length. Equation (1) gives an expression for the natural frequencies of a submerged beam or cable with pinned ends and under constant tension showing the effect of the added mass coefficient;

$$\omega_{n,\text{fluid}} = [(n\pi/L)^2 T + (n\pi/L)^4 EI]^{1/2} [\rho_f D^2 (\mu + \pi C_a/4)]^{-1/2}, \tag{1}$$

where L = length, T = tension, μ = mass ratio = $m/\rho_f D^2$, m = mass per unit length without added mass, C_a = added mass coefficient, E = Young's modulus, I = area moment of inertia of the beam, n = mode number, D = diameter, and ρ_f = fluid density.

When the added mass coefficient is zero, equation (1) yields the in-air natural frequency, $\omega_{n,\text{air}}$. The above expression for the submerged natural frequencies may also be expressed as the product of the in-air natural frequencies and a simple function of the added mass coefficient, as follows:

$$\omega_{n,\text{fluid}} = \omega_{n,\text{air}} [1 + (\pi C_a/4\mu)]^{-1/2}. \tag{2}$$

This equation may be solved for the added mass coefficient, C_a. By substituting the values of experimentally observed vibration frequencies in this expression, one may calculate the effective added mass coefficient. This was the objective of a set of experiments recently conducted by Chung (1989); he measured the self-excited cross-flow response amplitude and frequency for five flexible cylinders in water with mass ratios varying from 1·6 to 6·1. The experiment was conducted in the recirculating cavitation tunnel of the Korea Research Institute of Ships and Ocean Engineering. The cylinders were 6·0 mm in diameter and 0·6 m long. His response amplitude versus reduced velocity data were consistent, as expected, with the behavior shown in Figure 4: that is lower mass ratio cylinders have broader lock-in bandwidths than high mass

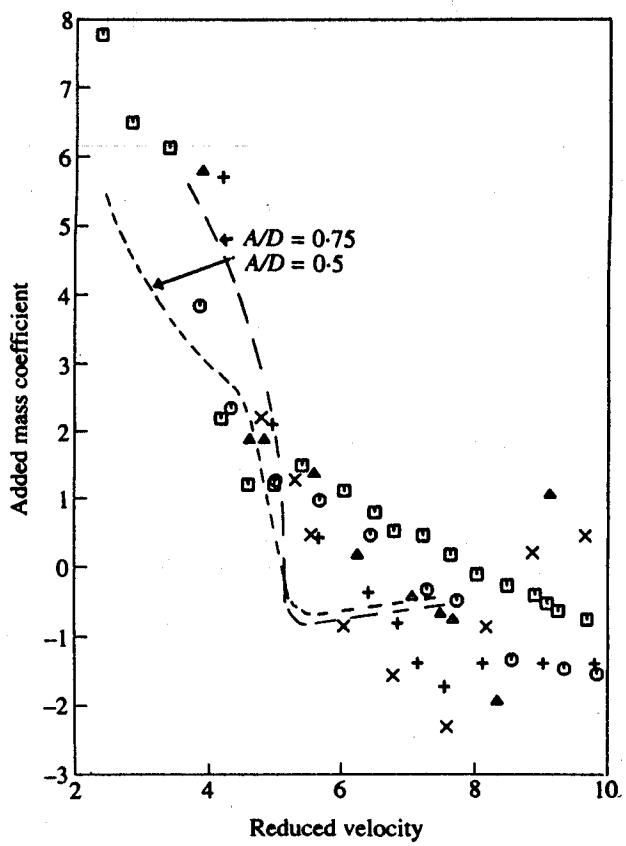

Figure 5. Effective added mass coefficient versus reduced velocity (Chung 1989 & Sarpkaya 1977): □, rod 1, $m/\rho_f D^2 = 1{\cdot}6$; ○, rod 2, $m/\rho_f D^2 = 2{\cdot}6$; Δ, rod 3, $m/\rho_f D^2 = 3{\cdot}3$; +, rod 4, $m/\rho_f D^2 = 5{\cdot}0$; ×, rod 5, $m\rho_f D^2 = 6{\cdot}1$.

ratio ones. He used the observed vibration frequency data to calculate effective added mass coefficients. These are plotted versus reduced velocity in Figure 5. Also plotted in the figure are the added mass curves (Sarpkaya 1977) for amplitude to diameter ratios of 0·5 and 0·75. The amplitude of vibration of the experimental cylinders was in the form of the half sine wave mode shape of the first mode of vibration, and therefore, varied from 0·0 at the ends to a maximum at the midspan. The midspan amplitude varied with reduced velocity in the lock-in range from 0·2 to 1·3 diameters. Since Sarpkaya's data show that the added mass is sensitive to amplitude, then Chung's results reflect an effective aggregate added mass, which represents a form of spatial average of the local added mass. Furthermore, for each reduced velocity the peak amplitude of Chung's test cylinders was different. Therefore, it is not possible to make a one-to-one comparison between the Sarpkaya curves and the calculated effective added mass coefficients. Nonetheless, the similarity between Chung's effective added mass coefficients and Sarpkaya's data supports the theory that variation in added mass allows the natural frequency to rise with flow speed.

The effect of mass ratio, as presented above, must be taken into account when predicting the likelihood of lock-in response of flexible cylinders in uniform flows. For example, tensioned cables with negligible bending stiffness have uniformly spaced natural frequencies. For each natural frequency there is a range of flow speeds which may permit lock-in. The width of this range is governed by the mass ratio. Low mass ratio will result in large variation in natural frequency and thus cause the overlap of the lock-in range of each natural mode with the neighboring modes. This was the case with the cable tested at Castine in 1981, and described earlier. The cable had a specific

gravity of 1·408 ($\mu = 1{\cdot}106$). Judging from the data in Figure 4, such a cable would be able to lock-in over a range of reduced velocities from approximately 4 to 8. This corresponds to a doubling in flow velocity. Thus, the lock-in range of the first mode of the cable extended to the range of the second mode, which had an in-air natural frequency twice that of the first mode. Similarly, the second, third and higher modes had overlapping lock-in regions. The cable tested at Castine was able to lock-in at all flow speeds, with typical response amplitudes of ±1 diameter at the antinodes.

Since the natural frequencies are uniformly spaced for a constant tension cable, the overlap of the modes becomes greater at higher mode numbers. At the tenth mode, a lock-in bandwidth of less than ±10% would overlap the lock-in bands of the 9th and 11th modes. Thus, all constant tension cables, independent of mass ratio, will have overlapping lock-in ranges for mode numbers exceeding the tenth mode, and many cables with low mass ratio will have overlapping lock-in ranges at much lower mode numbers.

Beams under tension behave differently. At low mode numbers, tension effects may be dominant, and the natural frequencies may be similar to those of cables, as one can deduce from equation (1). At higher mode numbers, however, the bending effects become important. When the bending effects are dominant, the natural frequencies increase as n^2, and the separation between natural frequencies increases in proportion to $2n$. Thus for beams under tension, if the lock-in regions do not overlap for low model frequencies, they probably will not at high mode numbers.

The pipe tested at Castine experienced lock-in at its first four natural frequencies, as dictated by the flow speed. The lock-in regions did not overlap, and as flow speed increased the pipe exhibited clearly defined ranges of lock-in and nonlock-in behavior. The lock-in ranges did not overlap. This was not because the pipe had greater separation between natural frequencies than did the cable. In fact, the first four excited modes for both the pipe and cable had quite similar in-air natural frequencies. For example, the first five natural frequencies for the cable at 792 lb. (3523 N) tension were 1·20, 2·39, 3·58, 4·79 and 6·08 Hz. For the pipe at 1,000 lb. (4448 N) tension the first five natural frequencies were 0·86, 1·77, 2·86, 4·26 and 5·73 Hz. The clear lack in the overlap of the lock-in regions for the pipe was primarily due to difference in mass ratio. The specific gravity of the pipe was 2·4 ($\mu = 1{\cdot}89$), and it was, therefore, less sensitive to changes in added mass than was the cable, which had a specific gravity of 1·41. As a consequence the pipe had a narrower lock-in range than the cable, permitting the existence of nonlock-in regions between lock-in ones.

As biaxial accelerometers were used it was possible to observe both the cross-flow and in-line response of the cable and pipe. It was discovered that the in-line response was highly correlated to the cross flow, especially under lock-in conditions. The correlation was non-linear and could be approximated by a square law model. This correlation is discussed in Vandiver & Jong (1987).

2.4. Reynolds Number Dependence

The Reynolds number range encountered in the tests at Castine was from zero to 10,000. Vibration was observed above approximately 300. From 300 to 10,000 the vibration behavior seemed to have little Reynolds number dependence. Cylinder motion appears to be more important than the Reynolds number in determining lock-in characteristics. Further evidence of this insensitivity of flow-induced vibration to Reynolds number may be found in numerous reports of the large amplitude vibration of drilling risers and pilings (Griffin & Ramberg 1982).

2.5. The Tolerance of Lock-In To Small Amounts of Shear

The 900 foot (274 m) long wire rope test: when two or more modes are within the lock-in range, one may dominate. The long wire rope tested in 1975 had at least ten modes potentially capable of lock-in. Somehow, one mode, approximately the 50th was able to dominate. This was in spite of the fact that the flow speed varied approximately 20% along the submerged portion of the cable. Lock-in was possible because a 20% variation in speed, and therefore reduced velocity, is within the tolerance of the wake to remain synchronized with a cylinder vibrating at one frequency. In this case the mode, which was, apparently, best positioned in frequency to lock-in over the entire length, dominated. As the tidal current slowly changed, the responding mode would change, interspersed with periods of random vibration, characteristic of nonlock-in behavior. The mode number was estimated by measuring the distance between vibration nodes, which were clearly visible on the portion of the cable which was not submerged.

A subtle question remains, regarding the relative importance of a sheared flow profile and mass ratio in determining the possibility of lock-in. Consider a low mass ratio cylinder with a reduced velocity lock-in range of 4 to 8, such as shown in Figure 4. If this cylinder were exposed from one end to the other to a sheared flow, such that the reduced velocity, based on the in-air natural frequency, varied from 4 to 8, would the cable be able to lock-in over the entire length? The answer is emphatically no. Although the added mass coefficient may vary along the length, the aggregate added mass on the cable results in a single resonant frequency for each mode and sheared flow profile. At any specific frequency, the lock-in tolerance bandwidth of the wake is of the order of 25% (i.e., $5 \leq V_R \leq 6{\cdot}5$), as previously revealed in numerous forced cylinder oscillation tests. Therefore, the wake synchronization regions of cylinders in sheared flows are restricted to zones over which the velocity varies by approximately 25%.

Is it then possible for a long cylinder in a sheared flow to be divided up into zones of 25% current variation, with each zone exhibiting lock-in with a different mode at a different natural frequency? Again the answer is no, because multiple frequency components in the response are sufficient to prevent lock-in, as discussed in the next section. It is not possible for more than one mode at a time to synchronize with the wake.

It is possible for one mode to dominate the response through lock-in over that subsection of the cylinder which has a reduced velocity in the lock-in range for that mode. Those portions of the cylinder which lie outside of the lock-in range for that mode will provide hydrodynamic damping for the cylinder. In this way lock-in may occur even when the variation in the velocity exceeds 25%. In cases like this the vortex shedding in the outlying regions of the cylinder does not generate sufficient response amplitude at other frequencies to disrupt the wake synchronization in the lock-in region.

2.6. The Effect of Irregular Cylinder Motion on Lock-In

In the late 1970s, a likely lock-in prevention mechanism, which had not been previously studied, was irregular motion of the cylinder. A laboratory experiment was conducted to test the hypothesis that the introduction of a small amount of random cylinder motion, while maintaining a mean frequency most favorable to lock-in, could in fact prevent wake synchronization and lock-in. A set of driven cylinder experiments were conducted on a rigid cylinder 0·5 in (1·27 cm) in diameter and 20 in (50·8 cm) long in

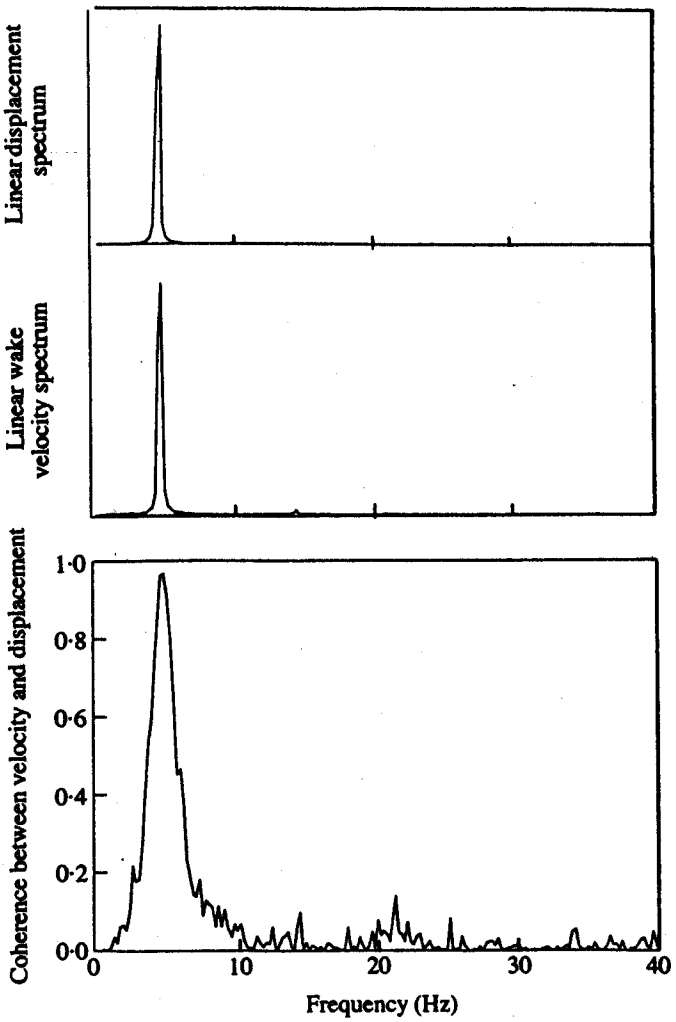

Figure 6. Displacement spectrum, wake velocity spectrum and coherence for sinusoidal lock-in conditions; $\mathrm{Re} \simeq 5000$, $A_{\mathrm{rms}}/D = 0{\cdot}109$.

the MIT Ocean Engineering Department's circulating water tunnel. The cylinder was driven in cross-flow vibration by an electromagnetic shaker. The cylinder vibration amplitude and spectral shape were varied in a controlled fashion. Three spectral shapes were used: sinusoidal, narrow-band random and broad-band random. All three had the same mean frequency. Flow velocity, hence reduced velocity, was systematically varied. Cylinder motion and drag force were measured. Wake velocity components were measured with a laser Doppler anemometer.

Under sinusoidal lock-in conditions, near-unity coherence was observed between wake velocity measurements and cylinder motion (Figure 6). However, when the cylinder motion was changed to a narrow-band random process with a center frequency the same as would usually result in lock-in, the coherence between cylinder motion and wake velocity dropped (Figure 7). Broad-band cylinder vibration reduced the coherence to near zero. The mean drag coefficient was also measured. The disruption in the lock-in process by random motions of the cylinder caused 50% reductions in drag coefficient (Shargel 1980). The principal limitation of the experiment was the lack of a systematic gradual variation in the bandwidth and r.m.s. amplitude of the vibration, for the purpose of establishing the boundaries of the lock-in phenomena.

An important conclusion to be drawn from these experiments is that lock-in is a

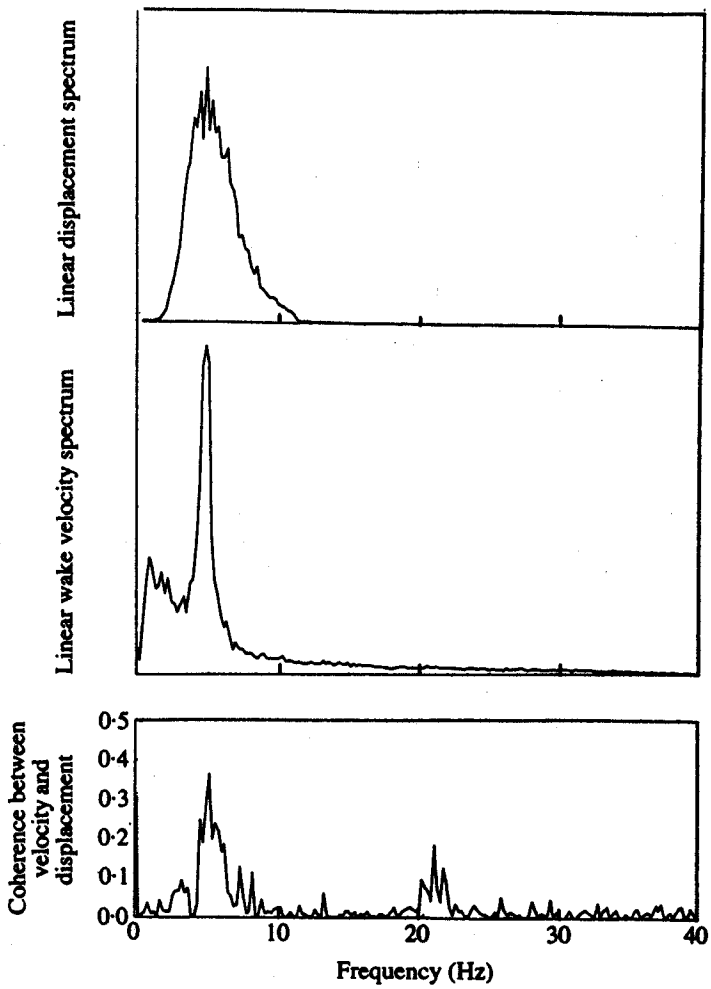

Figure 7. Displacement spectrum, wake velocity spectrum, and coherence for narrow band oscillations: $\mathrm{Re} \simeq 5000$, $A_{rms}/D = 0{\cdot}106$.

rather fragile phenomenon which can be reduced or prevented by vibration frequency components not at the lock-in frequency. An application of considerable significance is the response prediction problem in sheared flow. Vibration, generated at one location and with a particular frequency, may propagate to another, where the local flow velocity, hence lock-in frequency range, is different. The existence of the foreign-generated frequency components in the local vibration response, may be sufficient to prevent lock-in.

The maximum shear which can be tolerated and yet allows a cylinder to respond in a locked-in fashion is not known. It is probably very dependent on whether or not a second resonant frequency is included in the bandwidth of shedding frequencies which could be created by the given profile. If only one resonance is possible, then lock-in is likely, even with a rather large variation in the velocity profile. In this condition, the cylinder would lock-in over as much of the length as allowed by the lock-in bandwidth of the wake, which typically corresponds to a variation in flow velocity of about 25%. The remainder of the cylinder would be in an unsynchronized region providing additional damping. A common example of such a phenomena is the case of vertical pilings exposed to tidal flow, with large variations in the flow profile over the length. Large first-mode response dominates. The second mode natural frequency is typically outside of the vortex-shedding range, resulting in insufficient high frequency response

components to disrupt the first mode lock-in of the piling. In such cases, the additional damping contributed by the nonlock-in regions is not sufficient to prevent lock-in. Damping is important, however, and is discussed next.

2.7. The Reduced Damping Parameter

Response amplitude prediction under lock-in conditions has long been based on a dimensionless parameter known variously as the "reduced damping", the "stability parameter", or simply the "response parameter". This is sometimes written as S_G or ζ/μ, and defined as (Griffin & Ramberg 1982)

$$\zeta/\mu \equiv S_G \equiv 2\pi S_t^2(2m\delta/\rho_f D^2), \tag{3}$$

where $\delta = 2\pi\zeta$, the logarithmic decrement; $2\pi S_t = \omega D/V$; and, $\zeta = r/(2\omega m)$, the damping ratio.

The last expression assumes that the damping constant per unit length, r, is uniformly distributed along the cylinder. If this is not the case, one may replace r and m in the above expression by the modal damping and modal mass constants which can be computed by the techniques of modal analysis.

The reduced damping parameter is both useful and very often misinterpreted. As this parameter increases, response decreases. From equation (3) one can see that S_G becomes large for large values of damping ratio or for small values of mass ratio. The common erroneous conclusion is that low-density cables, hence cables with small mass ratio, are likely to respond more than high density ones. In fact, mass ratio has little to do with the response amplitude. When one replaces the Strouhal number, the damping ratio, and the mass ratio, in equation (3) with the definitions given, the following expression for S_G results:

$$S_G = r\omega/(\rho_f V^2), \tag{4}$$

which is independent of cylinder mass. S_G is essentially the ratio of dissipative forces on the cable to hydrodynamic exciting forces. It is a statement of dynamic equilibrium between the average power injected into the cable by the fluid through lift forces and the power dissipated by damping. Such a power flow equilibrium exists for all cases of vortex-induced vibration, including structures excited by sheared flow. One must, however, properly account for the hydrodynamic and structural sources of damping in each case, and must also properly account for the fluid excitation regions on the structure. This topic is discussed in some detail in Vandiver (1985).

If one wishes to use the reduced damping parameter to estimate response amplitude under lock-in conditions, then one must measure or estimate the correct damping. If the cylinder is expected to lock-in over its entire length, then the appropriate damping is the damping which one would measure in an *in vacuo* transient decay test. This is often called the structural damping and when expressed as a fraction of the critical damping ratio is written as ζ_s. For cylinders immersed in water, it is sufficiently accurate to use the structural damping ratio measured in air.

At Castine, the in-air measured damping ratios for the 2nd, 3rd, and 4th modes of the cable were $0{\cdot}002 \pm 0{\cdot}0005$ at a vibration amplitude of one diameter. For the pipe the damping ratios for the same modes were 0·002, 0·0015, and 0·001, with an accuracy of $\pm 0{\cdot}0005$. Hence, for the pipe and cable at low mode numbers the reduced damping did not exceed 0·002. Thus, on the basis of much empirical data, one would expect that the lock-in response amplitude for these cylinders would be approximately ±1 diameter at the antinodes, as was observed.

There are instances of lock-in when one must include some hydrodynamic damping in the reduced damping calculation. These correspond to lock-in conditions that do not include the entire length of the structure, such as the example of the piling excited by a tidal flow. Another example might be a layered flow, in which a uniform flow exists over a portion of a cable, and the reminder of the cable is immersed in stationary fluid. Hydrodynamic damping must be included for the portion of the cable in the stationary fluid. Though such an example is admittedly contrived, such conditions exist in experimental facilities equipped with flow channels which pass over deep pits, used for testing long objects.

3. CONDITIONS FAVORABLE TO MULTIPLE MODE NONLOCK-IN BEHAVIOR

3.1. Sheared Flow Experiments in the Arctic and St Croix

In 1982, a controversy developed within U.S. Navy circles regarding the correct drag coefficient to use in the design of very long mooring cables exposed to realistic, sheared, ocean currents. Was it necessary as a design precaution to use drag coefficients measured under lock-in conditions or were the reduced drag coefficients seen in the presence of random vibration more appropriate? In a strongly sheared current, would lock-in ever occur?

In 1983, two experiments were conducted on long, small diameter cables with the purpose of resolving the controversy. A shakedown experiment was first conducted on a vertical cable hung through the ice in the Arctic. Six months later a much more elaborate experiment was conducted from a U.S. Navy barge at St Croix in the U.S. Virgin Islands. A braided Kevlar cable 0·16 in. (0·406 cm) in diameter was hung vertically at lengths up to 2,000 ft (610 m) under tensions of approximately 20 lb. (89 N). A 0·094 in. (0·239 cm) Kevlar cable was also tested at lengths up to 9,000 feet (2,743 m). The current varied from a maximum of about 1·1 ft/s (0·335 m/s) at the surface to a minimum of approximately 0·1 ft/s (0·03 m/s) at depth, with substantial variations in between. Lock-in never occurred. Broad-band random vibration did occur, as can be seen in Figure 8. Accelerometer measurements, made as little as 275 ft (84 m) apart, were uncorrelated as shown in Figure 8. The cables responded to the vortex shedding as if they were of infinite length (Kim *et al.* 1985).

The uncorrelated response between the two locations could only be explained by invoking a total effective damping on the cable of 1·0 to 1·5% of critical, ten times the value of the measured structural damping. This observation was the first clear evidence that an important property of multi-moded, nonlock-in response was a large hydrodynamic damping component. Hydrodynamic damping prediction is addressed more fully later in this paper.

Drag coefficients, deduced from top tension and angle measurements, were found to be approximately 1·5. The corresponding rigid cylinder value in the Reynolds number range of 200 to 2,000 is about 1·2. High drag coefficients, typical of lock-in conditions, were never observed. R.m.s. response amplitudes of $\frac{1}{4}$ to $\frac{1}{2}$ diameter were observed. For these particular cables and shear conditions, the controversy was resolved. To generalize the observations requires the specification of appropriate dimensionless parameters, which can be used to predict the variations of response: from single mode lock-in, seen in the Castine experiments, to the broad band infinite cable behavior characteristic of the St Croix experiments.

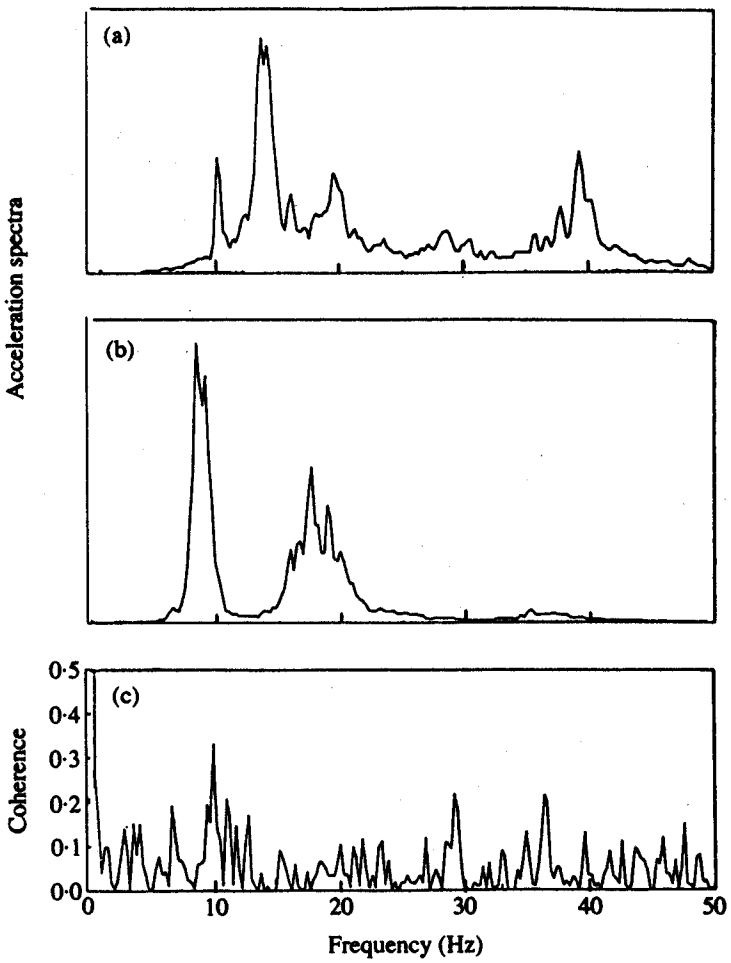

Figure 8. Acceleration spectra and coherence for two locations separated by 275 feet (83·8 m) (Kim *et al.* 1986): (a) acceleration spectrum 75 ft (22·86 m) below the surface; (b) acceleration spectrum 350 ft (106·7 m) below the surface; (c) coherence. Total cable length, 950 ft (289·6 m).

3.2. Useful Dimensionless Parameters

In the author's opinion the two most useful parameters for predicting whether or not lock-in will occur under sheared flow conditions are the number of natural modes contained in the bandwidth of vortex-shedding frequencies, hereafter referred to as N_s, and the dimensionless shear fraction, $\Delta V/V_{max}$. Other parameters may also be influential, though generally of secondary importance. For example, in some unusual circumstances the turbulence intensity may be large enough to prevent lock-in. Unusually high structural damping would also reduce the probability of lock-in under sheared flow conditions.

When it has been established that lock-in is not likely to occur and that the response will be dominated by the simultaneous contributions of many modes, then further consideration must be given to the role of hydrodynamic damping, because it is important in determining the nonlock-in dynamic response characteristics of the cylinder. At times, wave propagation effects, characteristic of an infinite cylinder, are dominant. Under other conditions, standing waves, characteristic of short resonant systems, are dominant. A wave propagation parameter, $n\zeta_n$, has proven to be a key to anticipating such behavior.

Thus, one determines if the necessary conditions are met to create multiple mode nonlock-in response, by evaluating the shear fraction and the number of excited modes

If the necessary conditions are met, one is then able to predict the dynamic characteristics of the cylinder, by evaluating the product of the damping (including hydrodynamic contributions) and the mode number, yielding $n\zeta_n$.

3.3. Shear Fraction and the Number of Excited Modes

It has previously been discussed that lock-in is most likely to occur, when the frequency bandwidth of the lift forces includes only one system natural frequency. The excitation bandwidth is strongly influenced by the severity of the shear, because of the relationship between flow velocity and vortex-shedding frequency. In this paper this excitation bandwidth is deduced primarily from the shear fraction, $\Delta V/V_{max}$. The excitation bandwidth is also influenced by the turbulence intensity level, V_{rms}/V_{max}, although it is usually of less importance. For a given excitation bandwidth, the number of modes likely to be included in the band is governed by the modal density of the natural frequencies of the cylinder. The spacing between frequencies depends primarily upon the mechanical properties of the system such as mass per unit length, stiffness, tension, and length. For example, the modal density of a constant tension cable is $1/f_1$ modes per Hz, or $1/\omega_1$ modes per rad/s, where f_1 is the first mode natural frequency of a taut cable.

One measure of the likelihood of lock-in is then given by the product of the excitation bandwidth and the modal density. This product is simply the number of natural frequencies contained within the excitation bandwidth, and is here defined as N_s (Kim *et al.* 1986).

The excitation bandwidth, Δf(Hz), due to sheared flow can be estimated using a reduced velocity value of approximately 5·9 and the variation in the velocity over the total length of the cylinder, ΔV, yielding

$$\Delta f = \Delta V/(V_R D). \tag{5}$$

The reduced velocity value of 5·9 is used, because it represents the average value observed under field conditions for a variety of flexible cylinders.

For the constant tension cable, N_s, the potential number of responding modes, is given by

$$N_s = \Delta f/f_1 = \Delta V/(f_1 D V_R) = 0{\cdot}17\Delta V/(f_1 D) \tag{6}$$

One must consider the size of this number and the shear fraction, $\Delta V/V_{max}$, when determining whether or not lock-in will occur. Three experimental examples are discussed here: the 950 ft (290 m) long cable tested at St Croix, the short 75 ft (22·9 m) long cable tested at Castine, Maine in 1981, and the 900 ft (274 m) long wire rope tested at Castine in 1975.

3.3.1 *The St Croix cable*

The velocity variation at St Croix was approximately 1·0 ft/s (0·3 m/s), yielding a shear fraction of $\Delta V/V_{max} = 0{\cdot}91$. A 91% variation in flow velocity is much larger than the approximately 25% maximum lock-in bandwidth which can be tolerated by the wake. On this evidence alone, one might suspect that lock-in might not occur. However, the number of modes potentially excited by this shear profile should also be estimated. The modal density, $1/f_1$, for the 0·16 in. (0·406 cm) diameter Kevlar cable at a length of

950 ft (290 m) and a tension of 21 lb (93·4 N) was 10·6 modes/Hz. Letting $V_R = 5{\cdot}9$, N_s, the number of simultaneously excited modes, is found to be 135. Lock-in was never observed. Infinite cable behavior was observed.

3.3.2 *The Castine cable, 1981*

This cable is described in detail in Table 1. At 350 lb. (1557 N) tension, this 75 ft (22·9 m) long, $1\frac{1}{4}$ in. (3·17 cm) diameter cable had a modal density, $1/f_1$, of 1·0 mode/Hz. The maximum current at Castine was approximately 2·5 ft/s (0·762 m/s) with a spatial variation of approximately 6%, measured over the length of the test section. This yields a ΔV of approximately 0·15 ft/s (0·046 m/s) and a variation in shedding frequency, as computed from equation (5) of 0·24 Hz. The turbulence intensity level was also very low; less than 5%.

For this case, $N_s = 0{\cdot}24$, for $V_R = 5{\cdot}9$. As a consequence, lock-in was frequently observed at Castine. It happened whenever the mean flow velocity resulted in a shedding frequency which coincided closely with a natural frequency. This happened almost all of the time for the cable due to added mass variations as discussed before.

Had the above calculation been done for the pipe tested at Castine, the result would have been almost identical, because for the modes excited at Castine the pipe had almost the same modal density as the cable. However, non-resonant, nonlock-in response did occur when the mean shedding frequency fell outside the lock-in bandwidth of any one natural frequency. Under lock-in conditions, the lift force is periodic and the excitation bandwidth is very narrow. Under nonlock-in conditions, even with very uniform flow, the lift force excitation spectral bandwidth broadens substantially, and the lift force and resulting cylinder response are best characterized as random processes.

Note that N_s approaches zero as the incoming flow becomes uniform. When N_s is less than one, the possibility of exciting a single natural mode of the cable is very high, and single mode lock-in is very likely. Alternatively, if N_s is very large, there is little chance to have lock-in, as more than one mode is always involved in the response. For the St Croix test, N_s was greater than 100, and lock-in never occurred.

3.3.3. *The Castine, 1976, 900 ft (274 m) wire rope*

Between the two extremes described above, the prediction of the occurrence of lock-in is not so clear. The 0·280 in. (0·711 cm) diameter, 900 ft (274 m) long wire rope, tested at Castine in 1976, is a good example. The relevant data are given in Table 2. The modal density for this case was 5·24 modes/Hz (computed with $C_a = 1{\cdot}0$) and the shear

TABLE 2

Castine wire rope test

V_{max}	1·3 ft/s (0·396 m/s)
T	350 lb (1557 N)
D	0·280 in (0·711 cm)
ΔV	0·25 ft/s (0·076 m/s)
L	900 ft (274 m)
m	0·00211 slugs/ft in air = 0·0101 kg/m
ζ_s	0·001, structural modal damping ratio
V_{rms}/V_{max}	$\leq 0{\cdot}05$

fraction, $\Delta V/V_{max}$, was 0·2. Using a reduced velocity of 5·9, equations (5) and (6) yield an estimate for N_s of 9·9 modes.

In this case lock-in did frequently occur. Even though N_s, the number of potentially excited modes, was nearly 10, one mode at a time dominated. The circumstances were such that, much of the time, no factor intervened to prevent lock-in. The turbulence level was too low to interfere, and the structural damping was too low to prevent lock-in.

The shear fraction was the pivotal parameter in this case. The shear fraction of approximately 20% was within the permissible lock-in bandwidth of the wake, thus allowing lock-in to occur over the entire length of the cable with the most favorable mode. However, a review of the recorded data indicates that about half the time lock-in did not occur, suggesting that, had the shear been much greater in the experiment, lock-in would have been prevented.

3.4. The Boundary Between Lock-In And Nonlock-In

At this point the exact upper bound on lock-in bandwidth is not known. It was suggested by Griffin (1985) that the lock-in bandwidth might be as large as 70% of the natural frequency; he also introduced a parameter which serves the same purpose as N_s.

It has been shown by Stansby (1976) that lock-in can exist on short-driven cylinders with shear fractions greater than 20%. His test cylinders had L/D of 8 and 16. In his experiment the shear fraction was approximately 33% and, in one scenario, lock-in occurred over the entire length. However, his results show that the extent of the lock-in region in a sheared flow on a driven cylinder is very amplitude dependent, and is related to the formation of a single coherent vortex cell in the wake. In sheared flow the presence of vibration nodes on the cylinder and spatially varying amplitudes, suggests that such long lock-in regions will not occur on typical structures with large L/D and high mode number.

When lock-in occurs with one of the lowest modes of the structure, it may happen without wake synchronization over the entire structure. This is a very typical occurrence on cantilevers, which may exhibit very large tip deflections under lock-in conditions with the lowest frequency natural mode. With such cylinders there are often regions which are not locked-in and act as hydrodynamic damping regions. Although vortex shedding is happening in these nonlocked-in regions, the frequency of the resulting lift force does not correspond to any other system natural frequency, and the resulting small response amplitudes are not sufficient at these frequencies to disrupt the lock-in process.

For long cables and risers, which respond at higher mode numbers, nonlock-in regions generate lift forces which do coincide with other system natural frequencies, creating wide band response which may prevent pure lock-in response from occurring, even in portions of the cylinder with conditions favorable to lock-in. The example of the 900 ft (274 m) long cable at Castine is a data point which marks one of the boundaries of lock-in behavior. In that case, N_s was 10. It is expected that for other scenarios in which one holds $\Delta V/V_{max}$ constant and decreases N_s, the probability of lock-in with a single mode increases.

3.5. Variations on the Shear Parameter, β

A parameter which has been conspicuously missing from the earlier discussion is the shear parameter β, because in its commonly used form it has no meaningful physical

interpretation. It is usually defined as

$$\beta = \left(\frac{D}{V_{\text{ref}}}\right)\frac{dV}{dx}$$

$$= \left(\frac{D}{L}\right)\frac{\Delta V}{V_{\text{ref}}}, \text{ for linear shears,} \tag{7}$$

where V_{ref} is variously defined in the literature. Letting V_{ref} be $V_{\max}$ for the purposes of this discussion, then for linearly varying sheared flow profiles

$$\beta = \left(\frac{D}{L}\right)\frac{\Delta V}{V_{\max}}. \tag{8}$$

This is just the ratio of the shear fraction $\Delta V/V_{\max}$, which is directly useful to L/D, which has little impact, except when less than 20 to 30. The division by L/D actually obscures the useful information in $\Delta V/V_{\max}$. Neither parameter β or $\Delta V/V_{\max}$ contains information about the dynamic properties of the cable. Additional parameters such as N_s, the number of excited modes, and $n\zeta_n$, the wave propagation parameter, are necessary to describe structural dynamic behavior.

There is an alternative form of β which may prove to be of some use. Experiments have shown that in sheared flows vortices are shed in cells (e.g., Stansby 1976). The cell length and hence the correlation length of lift forces are likely to depend on the percentage or fractional change in local vortex-shedding frequency per diameter of position change along the axis of the cylinder. If we assume that on average the local vortex-shedding frequency is proportional to the local flow velocity, then the fractional change in shedding frequency per diameter may be expressed as the quantity $(D/\omega_s)(d\omega_s/dx)$. This allows us to express the shear parameter, β, in a slightly different form, β_x, which has significance on the local level; it is the fractional variation in shedding frequency per diameter,

$$\beta_x = \frac{D}{\omega_s}\frac{d\omega_s}{dx} = \frac{D}{V(x)}\frac{dV}{dx}. \tag{9}$$

When this parameter is small, one would expect long correlation lengths and long cells. Therefore in linear shears, one would expect to see longer cell lengths in the higher velocity regions. Many other factors influence the cell length, such as cylinder motion, Reynolds number and turbulence. Nevertheless, it is proposed that β_x, a local measure of shear steepness, is a useful measure of the influence of the shear on lift force correlation length for long cylinders with large L/D.

4. HYDRODYNAMIC DAMPING IS CRITICAL IN DETERMINING DYNAMIC BEHAVIOR

The structural damping for tensioned marine structures susceptible to flow-induced vibration is usually very small and for structures in water is rarely the deciding factor in the determination of whether or not lock-in occurs. However, when lock-in does not occur or occurs over only a portion of the structure, then hydrodynamic sources of

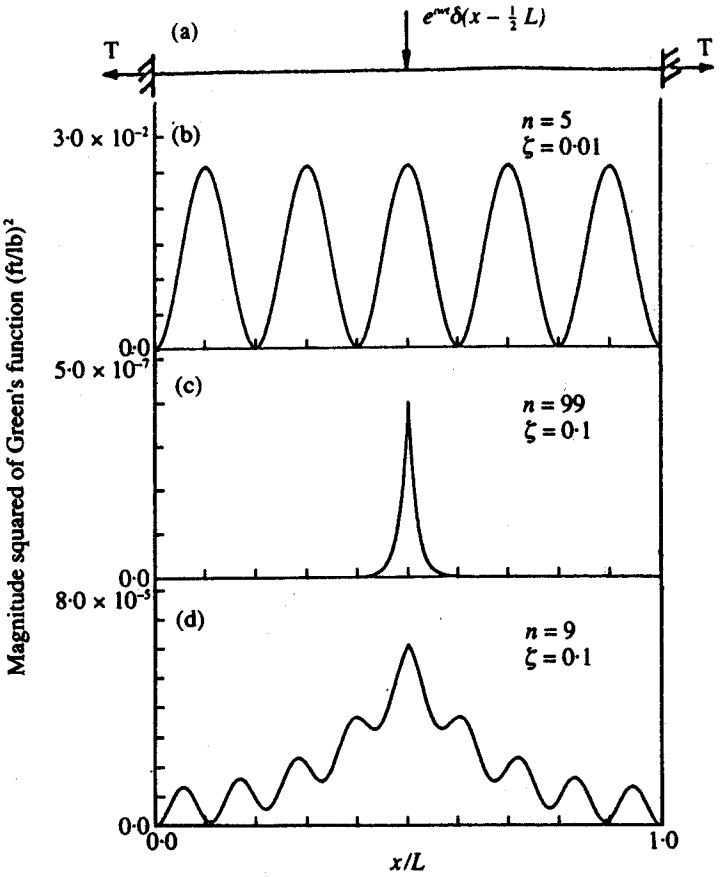

Figure 9. Magnitude of response to a unit harmonic force at $L/2$. (a) The system; (b–d) response Green's function.

damping can be large and become very important in determining dynamic response behavior. Whether or not a cable responds dynamically as if it is of infinite length or is dominated by standing waves depends heavily on hydrodynamic sources of damping.

4.1. How Long is Long?

The Green's function of a cable is the response of the cable to a unit harmonic exciting force at a specified location. Figure 9 shows the magnitude squared of the Green's function of a constant tension cable of length L to a unit harmonic force applied at its center, for three different values of the wave propagation parameter, $n\zeta_n$. Figure 9(b) shows the response when the excitation frequency is equal to the natural frequency of the 5th mode and the damping ratio is 1% of critical damping; $n\zeta_n$ is therefore 0·05.

The response shown is dominated by the standing wave mode shape for the 5th mode. Single mode resonant response dominates this case. A single mode approximation to the total response would be adequate. In Figure 9(c) the excitation frequency is equal to the 99th natural frequency and the damping ratio is 10% ($n\zeta_n = 9{\cdot}9$). The Green's function reveals that the vibration never reaches the cable ends. This is an example of infinite cable behavior. In Figure 9(d) the natural frequency of the 9th mode is equal to the excitation frequency and the damping ratio is again 10% ($n\zeta_n = 0{\cdot}9$). In this case the Green's function reveals a dynamic behavior between the first two extremes. Some attenuation of the response exists between the point of excitation and the ends of the cable. Some standing wave behavior is also exhibited.

The wave propagation parameter, $n\zeta_n$, may be used to predict which type of response is to be expected. This may be explained by considering a related parameter, $2L\zeta/\lambda$, where ζ is the damping ratio at the frequency of interest and L/λ is the ratio of the cylinder length to the average wavelength. Average wavelength is used to accommodate modest variations in tension. The reason that this parameter is relevant is that for linear damping, a wave travelling one length of the cable would decay by the factor $\exp(-2\pi\zeta L/\lambda)$. If the exponent $-2\pi\zeta L/\lambda$ is large and negative, then the attenuation is also large, and the response of the system will be like that of an infinite cable. When the exponent is small, little attenuation occurs, the exponential approaches 1·0, and standing wave resonant response would be typical. For the special cases of uniform cables and beams with pinned ends and constant tension, the factor $2L/\lambda$ equals the mode number, n and the parameter $2\zeta L/\lambda$ reduces to $n\zeta_n$, which is simply the product of the mode number and the damping ratio for that mode. In Figure 9, this parameter varies from 0·05 (standing wave with no apparent spatial attenuation) to 0·9 (strongly attenuated standing wave) to 9·9 (infinite cable response).

A recommended guide for interpreting the parameter $2\zeta L/\lambda$ or $n\zeta_n$ is as follows. When it is less than 0·2, clear standing wave behavior is to be expected over the entire cylinder. However, more than one mode may be present in the response. When it is greater than 2·0, then infinite cable behavior is the dominant characteristic. Between 0·2 and 2·0 this parameter implies that, at the frequency of interest, spatial attenuation will be important, but reflection from the ends will create a periodic modulation in the observed response of the cable, like that in Figure 9(d).

The terminations of cylinders which exhibit infinite cable characteristics deserve a special note. At the ends, reflections do occur, causing a local standing wave-like pattern, which attenuates rapidly with distance from the end.

The problem for the designer is to estimate both the mode number, n, and the damping ratio, ζ_n. The mode number or its equivalent, $2L/\lambda_n$, is relatively easy to obtain. The damping ratio, however, is not so obvious. Does one use structural damping or does one include the hydrodynamic sources of damping? This was a very controversial point in the mid- to late 1970s. At the time, most researchers, including the author, agreed that the structural non-hydrodynamic sources were the only important ones. When considering response in sheared flows that conclusion is completely false. The flaw is that in the 1970s the reasoning was narrowly focused on lock-in. Sheared flow phenomena were not being considered. Lock-in over the entire structure was the focus of most discussions. Under pure lock-in conditions the damping, which must be considered when evaluating the reduced damping parameter, is the structural damping. Under unusual conditions, lock-in may occur but not over the entire structure. In these cases, hydrodynamic damping from the nonlock-in regions should be included in the damping, when computing the reduced damping.

Under nonlock-in conditions in sheared flow, hydrodynamic damping must be considered, as it is often many times greater than the structural damping. This will be discussed in the next section.

4.2. Hydrodynamic Damping Estimation

A detailed hydrodynamic damping model is presented in Vandiver & Chung (1987). A simplified model, adequate for many applications is presented here. At any specific location, an instantaneous drag force per unit length may be defined as the force in the direction of the instantaneous relative fluid flow, as shown in Figure 10. The fluid

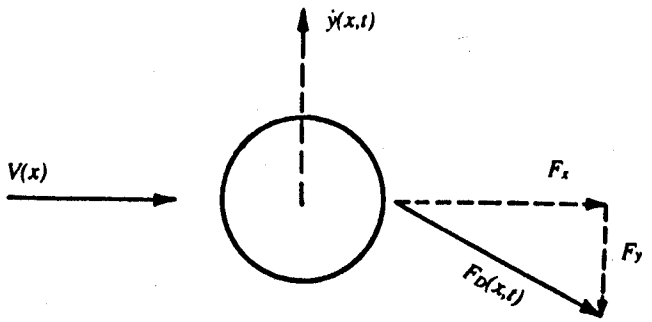

Figure 10. Damping force vector components.

velocity relative to the cable is the vector sum of the free-stream velocity, $V(x)$, and the negative of the local cross-flow cable velocity, $\dot{y}(x, t)$. The in-line cable velocity, $\dot{z}(x, t)$, is assumed to be small and is neglected (it could be included if greater precision was desired). If one assumes the drag force to be proportional to the relative velocity squared, then the magnitude of the drag force takes the form

$$F_D(x, t) = \tfrac{1}{2}\rho_f C_D D\{V^2 + \dot{y}^2\}. \tag{10}$$

Letting $B = \frac{1}{2}\rho_f C_D D$, the component of the drag force in the y or cross-flow direction is by simple trigonometry given by

$$F_y(x, t) = -B\dot{y}\{V^2 + \dot{y}^2\}^{1/2}. \tag{11}$$

The damping force in equation (11) is a nonlinear function of $\dot{y}$. It is helpful to find a linear equivalent damping constant, $r(x)$, which dissipates the same energy per cycle as the nonlinear one. This is the approach carried out explicitly in Vandiver & Chung (1987). However, under many conditions the following simplification is quite acceptable. When $V(x)^2 \gg \dot{y}^2$, then the cross-flow damping force per unit length reduces to

$$F_y(x, t) = -BV(x)\dot{y} = -r(x)\dot{y}, \tag{12}$$

where $r(x) = \frac{1}{2}\rho_f C_D D V(x)$. This is a simple linear damping model. The local damping ratio is then given by

$$\zeta = r(x)/[2\omega(m + \rho_f \pi D^2 C_a/4)], \tag{13}$$

where ω is the wave frequency on the cylinder. Substituting in for $r(x)$ yields

$$\zeta = \tfrac{1}{2}\rho_f C_D D V(x)/[2\omega(m + \rho_f \pi D^2 C_a/4)]. \tag{14}$$

The local velocity can be expressed in terms of a local Strouhal number and the local shedding frequency as follows:

$$V(x) = \omega_s D/(2\pi S_t). \tag{15}$$

Taking the example that the fluid is water, then the hydrodynamic damping ratio may be expressed as

$$\zeta_h = C_D \omega_s(x)/[2\pi^2 S_t \omega(\sigma_g + C_a)], \tag{16}$$

where σ_g is the specific gravity and ω is the vibration frequency. Strictly speaking, this is the local damping ratio for an infinite length cylinder. However, by using the techniques of modal analysis in Vandiver & Chung (1987), one may compute the modal damping ratio for a specific mode, n. In order to do this one must specify the shear profile. In the case of a linear shear profile the modal hydrodynamic damping ratio is given for mode n by

$$\zeta_{h,n} = C_D \omega_{s,\max} / [4\pi^2 S_t \omega_n (\sigma_g + C_a)], \tag{17}$$

where $\omega_{s,\max}$ is the maximum shedding frequency, corresponding to the peak flow velocity, and ω_n is the natural frequency of mode n. In the above two equations S_t was introduced so as to allow the local flow velocity to be expressed in terms of the local shedding frequency, $\omega_s(x)$. Therefore, S_t should be taken to have a value of about 0·17, which is the average value observed for moving cylinders in the field. This value, 0·17, is a refinement on the value of 0·2 used previously in Vandiver (1985) and Vandiver & Chung (1987).

These damping models were verified in a field experiment which is discussed in the next section of this paper. Prior to that discussion, it is important to consider one refinement of the modal damping model given in equation (17). Each excited mode will have a region of the cable where the local vortex-shedding frequency and the natural frequency coincide as depicted in Figure 11. In this region net power flows into that particular mode (Vandiver & Chung 1987). This region should be excluded in the calculation of hydrodynamic damping for that particular mode. This would cause a corresponding reduction in the damping ratio predicted by equation (17).

The precise delineation of these power input and damping exclusion ranges is at the present rather uncertain. It is discussed in Brooks (1987), Wang *et al.* (1988), and Vandiver & Chung (1987). The spatial extent of the damping exclusion region for each

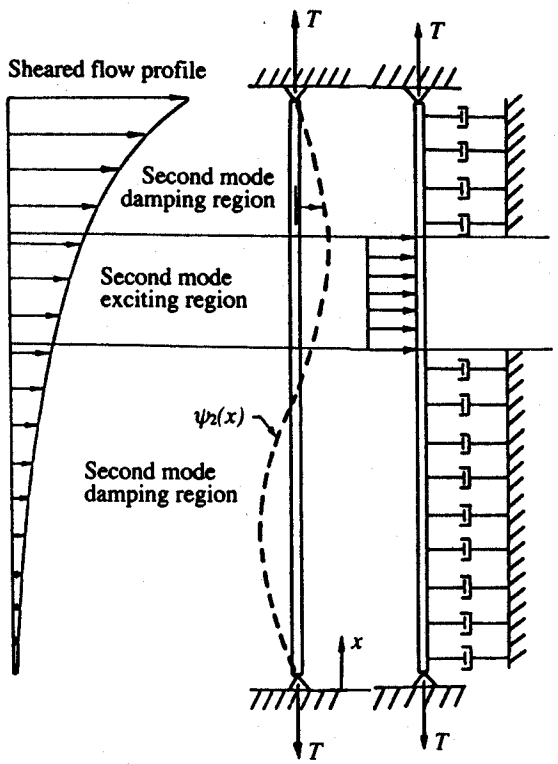

Figure 11. Power flow model for a flexible cylinder.

mode will decrease as the number of responding modes, N_s, increases. When N_s exceeds approximately 10, the magnitude of the correction to the estimated modal damping ratio, becomes sufficiently small that in most cases one needs not bother with it.

The assumption that $V(x)^2 \gg \dot{y}^2$ is not valid in the slow part of a stratified flow in which vibration from a high-velocity region passes suddenly into a region of very low or zero flow velocity. In the case of a region of zero flow, a different approximation may be used (Sarpkaya 1979).

As an alternative to the damping prediction model presented above, one may use measured lift coefficients determined in laboratory experiments. Gopalkrishnan (1993) presents contour plots of measured lift coefficient as a function of a wide range of reduced velocity and response amplitude. When the lift coefficients are negative they indicate damping.

A verification of the importance of hydrodynamic damping in sheared conditions was accomplished in a field experiment conducted in the summer of 1986, and reported on below.

5. THE SHEARED FLOW EXPERIMENTS AT LAWRENCE, 1986

The experiments were conducted for the purpose of validating the hydrodynamic damping model, and obtaining experimental data for the case that $n\zeta_n$ fell between the extremes of lightly damped individual modes, typical of the cables at Castine, and infinite cable behavior, typical of the cables tested in St Croix. At Castine in 1981, fourth mode lock-in vibration of the cable or pipe resulted in $n\zeta_n$ values of 0·008 and 0·004, respectively. Standing waves with no apparent attenuation were observed. For the St Croix experiments the total damping was approximately 1·5% and a typical value of $2\zeta L/\lambda$ was 2·3 at a length of 950 ft (290 m). Infinite cable behavior was observed.

The experiments were conducted during the summer of 1986. A complete description, including many figures, may be found in Chung (1987) and Vandiver & Chung (1987, 1988). The test site was a mill canal, built in 1848 in Lawrence, Massachusetts. A dam diverts the water from the Merrimack River into the canal. The flow is controlled by four submerged gates, which are spaced at equal horizontal intervals beneath a gate house at the head of the canal. By controlling the various gate openings a sheared flow can be developed horizontally across the width of the canal, which is approximately 58 feet (17·7 m). The average depth of the canal is 10 ft (3·05 m).

The test cable location was approximately 250 feet (76 m) downstream of the gate house. The cable was tensioned horizontally across the width of the canal about 1 ft (0·305 m) under the surface, as shown in Figure 12. Heavy steel pipe supports transferred the cable loads to the walls of the canal. Tension was applied to the cable via a system of pulleys and a hand-operated winch. For a given winch position the cable had essentially constant arc length. The tension then varied slowly with mean drag force on the cable. Tension was measured with a tension cell connected in series between the cable and winch.

Five feet (1·52 m) upstream of the test cable, a simple traversing mechanism was suspended from a taut wire above the waters of the canal to carry a Neil Brown Instruments DRCM-2, two-axis acoustic current meter. The transducer was located about 1 ft (0·305 m) underwater and was oriented so that the instantaneous velocity was resolved into two components in the horizontal plane. The velocity was measured at two samples per second.

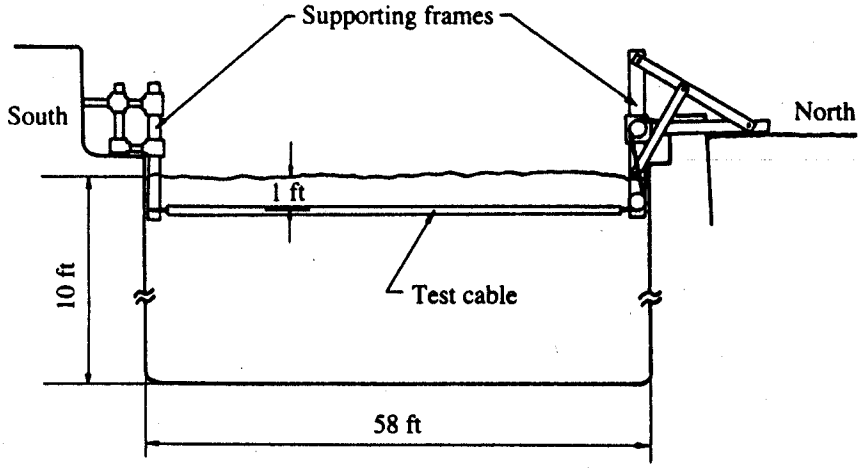

Figure 12. Lawrence test configuration, 1986.

The 58-ft (17·7 m) long test cable is shown in Figure 13. It consisted of a 1·125 in. (2·86 cm) rubber hose with a 0·5 in. (1·27 cm) inside diameter. Seven 0·16 in. (0·406 cm) diameter braided kevlar cables were carried inside the hose. Each kevlar cable had seven conductors inside it. Three kevlar cables were used solely as load-carrying members, three cables were used to carry accelerometer signals and power, and one cable was used as a spare.

Six biaxial pairs of force balance accelerometers were placed on the centerline of the cable at locations shown in the figure. Each biaxial pair was 0·5 in. (1·27 cm) in diameter and 3 in. (7·62 cm) long. Space was created for the kevlar cables to pass around the accelerometers at these locations, with no change in the outside diameter of the hose. The accelerometers, tension cell, and current meter were the same as those used in previous experiments conducted at Castine, Maine.

The 12 accelerometer outputs, tension, and current data were carried via a multi-conductor cable from the test cable to the gatehouse, where a Digital Equipment

(a) Location of accelerometers

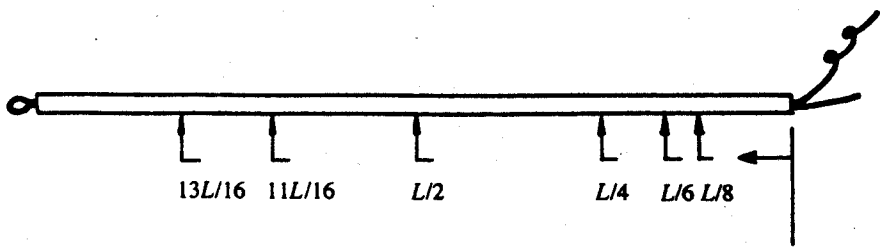

(b) Cross-section of test cable

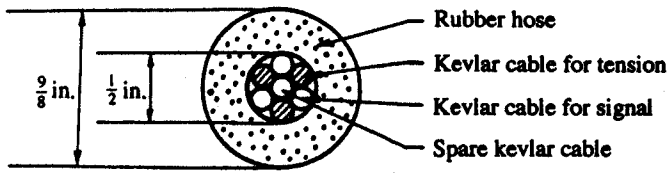

Figure 13. Lawrence test cable construction.

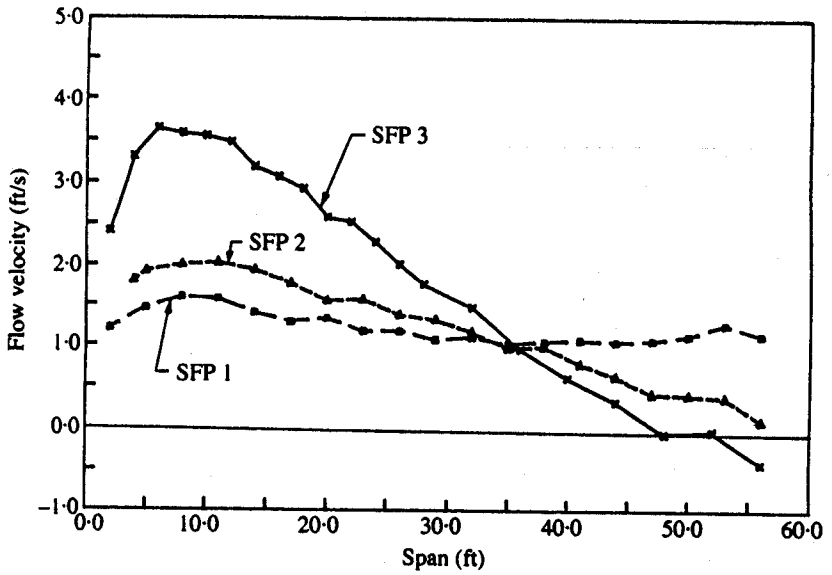

Figure 14. Shear flow profiles for the Lawrence experiments.

MINC-23 data acquisition computer was located. Fourteen data channels were digitized and stored on floppy disks.

5.1. Sheared Current Profiles

The current profiles were measured prior to response tests. The results of three different profiles are shown in Figure 14. They are designated shear flow profile 1, 2, and 3 (SFP1, etc.). SFP3 was the steepest shear with a peak flow velocity at times exceeding 4 ft/s (1·22 m/s) and a minimum flow velocity of −0·5 ft/(−0·152 m/s); the minus indicates reverse flow. SFP2, a milder shear, ranged from 2 ft/s (0·61 m/s) down to zero in a nearly linear profile. SFP1 was made as close to uniform as possible by careful positioning of the gates. The velocity varied approximately 30% along the length.

For all profiles, the flow was highly turbulent. The turbulence intensity level was from 10 to 20% of the maximum current in the profile. The longest time scale of the turbulence was up to several seconds in length, and was associated with large eddies, which were carried downstream from the gatehouse.

An important observation is that the turbulence was able to prevent constant-amplitude, single mode lock-in from occurring, even with the most uniform profile, SFP1, which had a $\Delta V/V_{max} = 0{\cdot}3$.

6. PREDICTED AND MEASURED HYDRODYNAMIC DAMPING

The structural damping measured by free vibration decay tests in air for the test cable in this experiment was about 0·3% of critical for the frequency ranges and tensions later experienced in the water. A more precise measure is not important because the hydrodynamic damping will be shown to be far larger.

Figure 15 is a sample time history of the response of the test cable in the highly

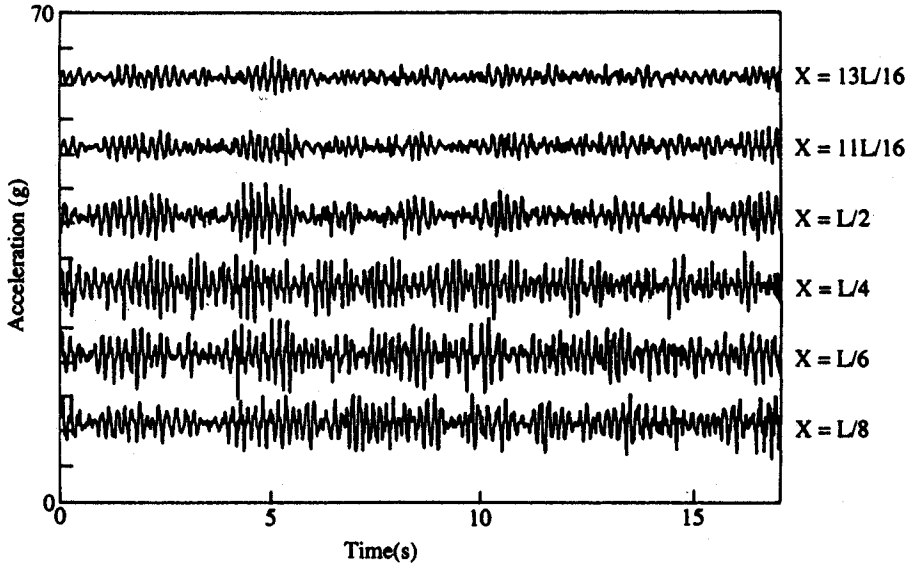

Figure 15. Cross-flow acceleration time histories for six accelerometer locations for the high shear profile, (SFP-3).

sheared flow, for which $\Delta V/V_{max}$ was 1·125. Simultaneous time histories of cross-flow acceleration are given for all six measurement locations. It is quite obvious that the high velocity locations had higher response than the low velocity regions. In this case the r.m.s. displacement was 0·3 diameters at $x = (13/16)L$ and 0·5 diameters at $x = L/8$. The tension was 151 lb. (672 N) and the natural modes were 0·6 Hz apart. The peak vortex-shedding frequency corresponded to about the 10th natural frequency, and therefore N_s, the number of excited modes, was approximately 10. Enough modes were involved in the response that variation in mode shape is not a particularly important factor when comparing the r.m.s. response of one location to another.

The decrease in observed r.m.s. response level between positions near opposite ends of the cable was only possible if $n\zeta_n$ was greater than 0·2. Structural damping alone with a value of $\zeta_s \simeq 0{\cdot}003$, leads to an estimate of $n\zeta_n$ for the 10th mode of 0·03; too small to explain the spatial attenuation. Hydrodynamic damping was important in this case and can be estimated using equation (17).

For this experiment, the specific gravity of the cable was 1·34. Letting the average added mass coefficient, C_a, and the drag coefficient, C_D, both be equal to 1·0, and setting S_t to a value of 0·17 leads to the following prediction for hydrodynamic modal damping ratios:

$$\zeta_{h,n} = 0{\cdot}064\omega_{s,max}/\omega_n. \tag{18}$$

The ratio $\omega_{s,max}/\omega_n$ is approximately equal to unity for the highest excited mode, independent of mode number. Therefore, for the highest excited mode, the hydrodynamic modal damping ratio is predicted to be 6·4%, which when added to the structural damping ratio yields a total damping of 6·7%. Since this was mode ten, then the parameter $n\zeta_n$ is 0·67. For the lower excited modes the hydrodynamic damping ratio is larger than 6·4% and increases in proportion to the ratio $\omega_{s,max}/\omega_n$. However, since n is smaller for lower modes, one finds that $n\zeta_n$ remains constant at 0·67. This value is as expected between the limits of 0·2 and 2·0 and consistent with the observed spatial attenuation in response.

To demonstrate conclusively that the predicted hydrodynamic damping is correct,

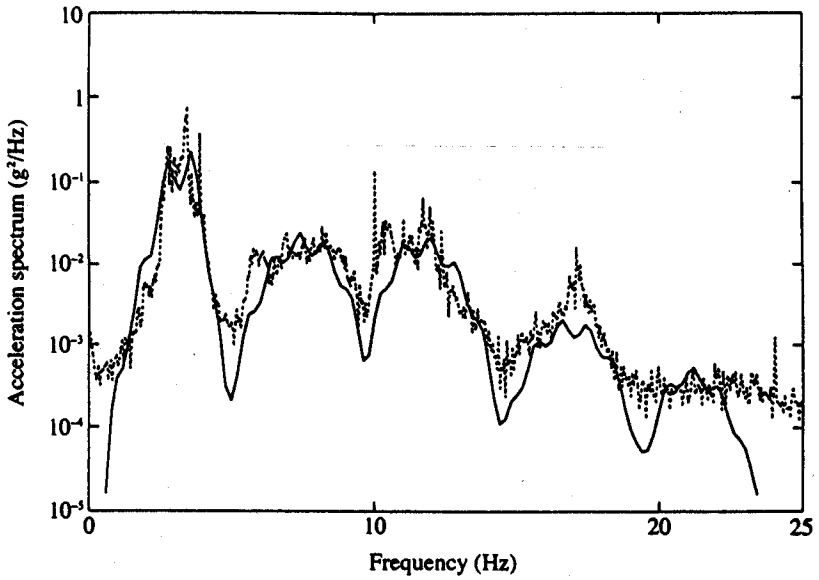

Figure 16. Measured and predicted acceleration response spectra at $13L/16$ (low current side) in profile SFP-2: ....., measured; ——, predicted.

one must use it in a prediction model which includes the effects of current shear and hydrodynamic damping. Such a model is proposed and used in Chung (1987) and Vandiver & Chung (1988). Comparisons between measured and predicted response for the sheared flow experiments at Lawrence are presented. One example is given here.

Figure 16 is a comparison between the predicted and measured acceleration response spectrum of the cable at $x = (13/16)L$. The cable was exposed to the intermediate shear profile (SFP2). The predictive model includes the effects of shear, turbulence, hydrodynamic damping, correlation length, and higher order harmonics of the vortex-shedding frequencies. For this case the maximum flow velocity was approximately 2·0 ft/s (0·61 m/s) and the highest excited mode was the fifth, with a predicted value of total damping of 6·7%. Again $n\zeta_n$ is constant and independent of mode number with a value of 0·33. The number of excited modes was five and $\Delta V/V_{max}$ was 100%. Lock-in was not observed. The controlling Green's functions for the cable had characteristics similar to those shown in Figure 9(d) and were consistent with values of $n\zeta_n$ equal to 0·3.

In summary, the Lawrence experiment provided an excellent opportunity to test the validity of using the dimensionless parameters recommended in this paper for predicting response characteristics. These parameters were N_s, $\Delta V/V_{max}$, and $n\zeta_n$, where ζ_n included hydrodynamic effects.

The Lawrence tests also provided an opportunity to conduct a simple direct comparison between predicted and observed infinite cable hydrodynamic damping, as discussed next.

6.1. Impulse Response under High Tension in a Turbulent Uniform Flow

With large hydrodynamic damping, the vibration excited at one location is attenuated as it travels through the cable to distant points. This was confirmed by an independent measurement. Under steady-state flow-induced vibration conditions, the cable was struck impulsively with a wooden pole, at a location near one end. An impulse

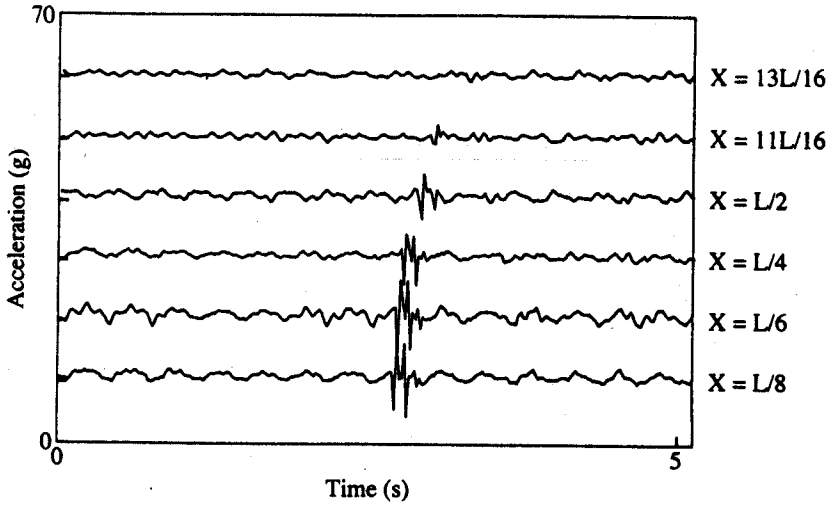

Figure 17. Measured impulse response propagation time histories.

propagated through the cable. Figure 17 shows the simultaneous time histories at all six accelerometer locations. The impulse can be seen to travel from one location to the next with a travel time delay and an attenuation due to damping. By comparing the spectra of the accelerometer time histories, it is possible to estimate the frequency content of the impulse and the effective damping coefficient. The cable tension was 450 lb. (2002 N), the current was the approximately uniform profile (SFP1), $\Delta V/V_{max} = 0{\cdot}3$. The flow-induced vibration response of the cable was dominated by nonlock-in third mode response at a natural frequency of 3·0 Hz and an r.m.s. response of approximately $\frac{1}{2}$ diameter. The predicted damping experienced by the impulse as it travelled along the cable may be obtained by using the damping model for waves travelling along an infinite cable. The infinite cable model is valid for the period of time prior to the reflection of the pulse from the far end of the cable. By using equation (16) and the following values for the necessary constants, the hydrodynamic damping prediction is obtained. Letting $C_D = 2{\cdot}0$, $S_t = 0{\cdot}17$, $C_a = 1{\cdot}0$, and $\sigma_g = 1{\cdot}34$, yields

$$\zeta_h = 0{\cdot}256\omega_s(x)/\omega. \tag{19}$$

The dominant shedding frequency was 3·0 Hz. The impulse had most of its energy in the 15 to 24 hz range. Taking 18 Hz as a frequency typical of the impulse, the above equation yields a hydrodynamic damping prediction of 4·3%. A C_D of 2·0 was used to reflect the relatively larger r.m.s. response (0·5 diameter).

If the damping behaves linearly, then the attenuation of the wave amplitude as a function of the distance travelled is given by

$$\text{attenuation} = e^{-\zeta kd} = e^{-\zeta\omega d/c}, \tag{20}$$

where $k = \omega/c$, the wave number; c = speed of wave propagation; and d = distance travelled.

Since response spectra are proportional to response amplitude squared, then the attenuation of the impulse energy in the 15 to 24 Hz band should be given by the square of the above equation. If A_1 and A_2 are the spectral magnitudes in the 15 to 24 Hz band for two different locations, a distance d apart, then the effective damping may be deduced by

$$\zeta = c\ \ln(A_2/A_1)/2\omega d. \tag{21}$$

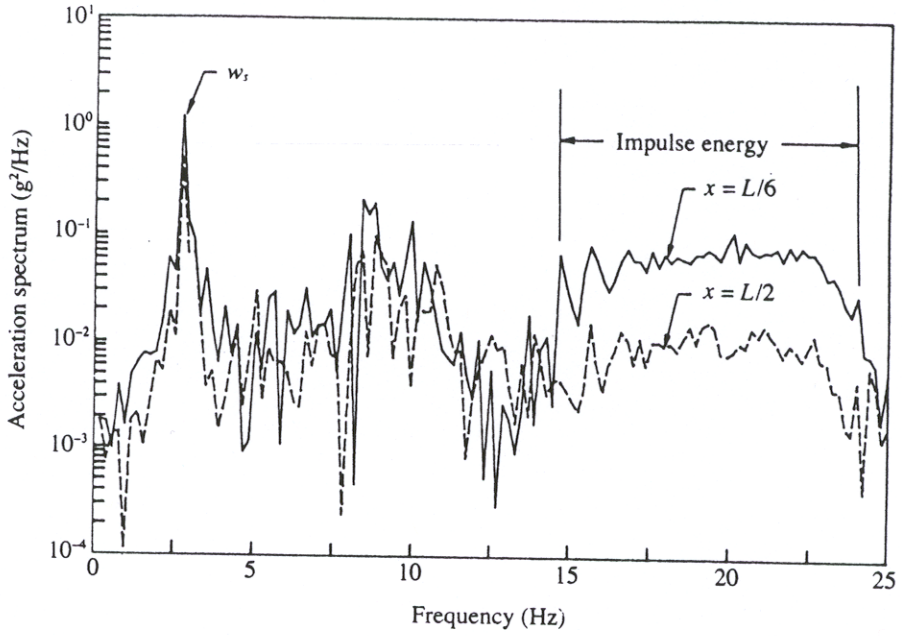

Figure 18. Measured impulse response spectra at $L/2$ and $L/6$ in a very turbulent uniform flow, profile SFP-1.

The two spectra in Figure 18 are used here as an example. The locations were separated by 19·3 ft (5·88 m). Choosing a typical frequency of $f = 18$ Hz, and noting that $\omega = 2\pi f$, $d = 19{\cdot}3$ ft (5·88 m), $c = 120$ ft/s (36·6 m/s), and the ratio of the two spectra in the 15 to 24 Hz band is approximately six to one, results in an estimate of $\zeta = 0{\cdot}049$ or 4·9% compared to the prediction of 4·6%. Many similar calculations were performed between different locations and for different impulse events. The results fell into a range of 4 to 6% total damping.

If one substitutes the formula for damping as given in equation (19) into equation (20) for wave attenuation, the result is independent of vibration frequency. This is consistent with the expression for damping ratio in equation (16), which states that damping ratio decreases with frequency. Over a fixed distance, d, high-frequency waves travel more wavelengths than low-frequency waves, which have greater damping but travel fewer wavelengths. Over a fixed distance all vibration frequency components attenuate the same amount.

7. SUMMARY AND CONCLUSIONS

The design of moorings, ROV tethers, pipelines, and petroleum drilling and production risers depends on the expected magnitude and frequency of vortex-induced vibration. Lock-in usually results in the largest amplitudes of vibration and the largest mean drag coefficients, and, therefore is considered in most situations to be the worst case. Establishing whether or not it will occur is usually of great concern. This paper has attempted to reveal those parameters which have greatest influence over the occurrence of lock-in for flexible cylinders with large L/D, and has provided case studies to support the conclusions.

The parameters most useful for determining whether or not lock-in will occur are the shear fraction, $\Delta V/V_{max}$, and the number of potentially excited modes, N_s, and to a usually lesser extent the turbulence intensity.

When lock-in is likely to occur, the mass ratio has a strong effect on determining the

range of reduced velocity over which lock-in can occur. If this range is narrow, then lock-in may occur only for narrow bands of flow velocity. For low mass ratio cylinders the reduced velocity lock-in range is broad and lock-in regions may overlap, such that transition from lock-in in one mode to the next is possible as the velocity increases.

Under lock-in conditions the response amplitude may be predicted using the response parameter, S_G, based on the structural damping and the hydrodynamic damping contributed from nonlock-in regions. However, S_G has been shown not to be a function of mass ratio as commonly believed.

Another parameter, $n\zeta_n$, has been shown to reveal whether standing waves or attenuated travelling waves dominate the nature of the dynamic response. Standing wave behavior is a necessary condition for lock-in to occur. In sheared flows which create nonlock-in dynamic response, hydrodynamic damping has been shown to be usually much more important than structural damping in governing response amplitude. Thus nonlock-in vibration in sheared flows is often accompanied by larger values of the parameter $n\zeta_n$, and spatially attenuated vibration is often observed.

Many conclusions require further refinement, largely through experimental work. In many cases the critical parameters are known, but the values which mark the transition from one type of behavior to another need refinement. For example, what combination of values of N_s, the number of potential responding modes, and $\Delta V/V_{max}$, the shear fraction, define the boundary between lock-in and nonlock-in? What is the effect of turbulence and temporal variations in mean flow speed? These and many other similar problems require experimental data before they can be resolved.

ACKNOWLEDGEMENTS

This research was supported by a consortium of government and industry sponsors. These sponsors included: Amoco, Chevron, Conoco, Exxon Production Research, Mobil, Petrobras, Shell Development Co., the Technology Assessment and Research Programme of the Minerals Management Service, and the MIT Sea Grant Programme under agreement number NA86AA-D-SG089.

References

Brooks, I. H. 1987 A pragmatic approach to vortex-induced vibrations of a drilling riser. In *Proceedings 1987 Offshore Technology Conference,* Paper OTC 5522, pp. 327–332; Houston, Texas, U.S.A.

Chung, T. Y. 1987 Vortex-induced vibration of flexible cylinders in sheared flows. Ph.D. dissertation, MIT Department of Ocean Engineering, Cambridge, Mass., U.S.A.

Chung, T. Y. 1989 Vortex-induced vibration of flexible cylinders having different mass ratios. Report No. UCE 440-1283ED, Korea Research Institute of Ships and Ocean Engineering.

Gopalkrishnan, R. 1993 Vortex-induced forces on oscillating bluff cylinders. Ph.D. dissertation, MIT Department of Ocean Engineering and Woods Hole Oceanographic Institution.

Griffin, O. M. 1985 The effects of current shear on vortex shedding. In *Proceedings Separated Flow Around Marine Structures,* pp. 91–110, Norwegian Institute of Technology, Trondheim, Norway.

Griffin, O. M. & Ramberg, S. E. 1982. Some recent studies of vortex shedding with applications to marine turbulars and risers. *ASME Journal of Energy Resources Technology* **104,** 2–13.

Griffin, O. M. & Vandiver, J. K. 1984 Vortex-induced strumming vibrations of marine cables with attached masses. *ASME Journal of Energy Resources Technology* **106,** 458–485.

Kim, Y. H., Vandiver, J. K. & Holler, R. 1985 Vortex-induced vibration and drag coefficients of long cables subjected to sheared flow", In *Proceedings 4th OMAE Symposium* **1,** pp. 584–592.

KIM, Y. H., VANDIVER, J. K. & HOLLER, R. 1986 Vortex-induced vibration and drag coefficients of long cables subjected to sheared flow. *ASME Journal of Energy Resources Technology* **108,** 73–83.

KOCH, S. 1985 Private communication of data from experiments conducted in a towing tank by Exxon Production Research.

PHAM, THAI Q. 1977 Evaluation of the performance of various strumming suppression devices on marine cables. Master's thesis, MIT Department of Ocean Engineering, Cambridge, Mass., U.S.A.

SARPKAYA, T. 1977 Transverse oscillations of a circular cylinder in uniform flow, Part I. Naval Postgraduate School Report No. NPS-69SL77071.

SARPKAYA, T. 1979 Vortex-induced oscillations: a selective review. *Journal of Applied Mechanics* **46,** 241–258.

SHARGEL, R. 1980 The drag coefficient for a randomly oscillating cylinder in a uniform flow. Master's Thesis, M.I.T. Department of Ocean Engineering, September 1980.

STANSBY, P. K. 1976 The locking-on of vortex shedding due to the cross-stream vibration of circular cylinders in uniform and shear flows. *Journal of Fluid Mechanics* **74,** 641–665.

TSAHALIS, D. T. 1984 Vortex-induced vibrations of a flexible cylinder near a plane boundary exposed to steady and wave-induced currents. *ASME Journal of Energy Resources Technology* **106,** 206–213.

VANDIVER, J. K. 1983 Drag coefficients of long flexible cylinders. In *Proceedings 1983 Offshore Technology Conference,* Paper OTC 4490, pp. 405–414; Houston, TX, U.S.A.

VANDIVER, J. K. 1985 The predictions of lock-in vibration on flexible cylinders in a sheared flow. In *Proceedings 1985 Offshore Technology Conference,* Paper OTC 5006, pp. 405–412, Houston, TX, U.S.A.

VANDIVER, J. K. & CHUNG, T. Y. 1988 Predicted and measured response of flexible cylinders in sheared flow. In *Proceedings Symposium on Flow-Induced Vibration and Noise,* Vol. 1 (eds M. P. Païdoussis, O. M. Griffin & C. Dalton), pp. 1–23. New York: ASME.

VANDIVER, J. K. & CHUNG, T. Y. 1989 Hydrodynamic damping on flexible cylinders in sheared flow. In *Proceedings 1987 Offshore Technology Conference,* paper OTC 5524, pp. 343–353, Houston, TX, U.S.A.; and *ASCE Journal of Waterway Port and Coastal Engineering* 1989, **115,** 154–171.

VANDIVER, J. K. & JONG, J.-Y. 1987 The relationship between in-line and cross-flow vortex-induced vibration of cylinders. *Journal of Fluids and Structures* **1,** 381–399.

VANDIVER, J. K. & MAZEL, C. H. 1976 A field study of vortex excited vibrations of marine cables. In *Proceedings 1976 Offshore Technology Conference* **I,** paper OTC 2491, pp. 701–710, Houston, TX, U.S.A.

WANG, E., WHITNEY, D. K., & NIKKEL, K. G. 1988 Vortex shedding response of long cylindrical structures in shear flow. *ASME Journal of Offshore Mechanics and Arctic Engineering* **110,** 24–31.

APPENDIX: NOMENCLATURE

B	velocity-squared damping coefficient
c	phase velocity of waves in the cable
D	cylinder diameter
k	wave number $= \omega/c$
L	the cylinder length
m	structural mass per unit length not including added mass
N_s	the number of modes within the shear bandwidth
$r(x)$	local linear equivalent damping coefficient
S_G	response parameter (reduced damping)
S_t	Strouhal number
T	tension
$V(x)$	flow velocity at x
V_{max}	peak velocity in a linear shear
V_{rms}	turbulence standard deviation
V_R	reduced velocity
x	response measurement point
$y(x, t)$	cross-flow response displacement

	ζ_n	damping ratio for mode n
	$\zeta_{h,n}$	hydrodynamic part of modal damping ratio
	$\zeta_{s,n}$	structural part of modal damping ratio
3	ρ_f	fluid density
	ρ_w	water density
	σ_g	specific gravity
	ω	vibration frequency (rad/s)
	ω_s	local mean vortex-shedding frequency
	ω_n	natural frequency of mode n
	ω_{max}	natural frequency closest to the peak shedding frequency